

1 **Interferon-Induced Transmembrane Protein 3 Blocks**
2 **Fusion of Diverse Enveloped Viruses by Locally Altering**
3 **Mechanical Properties of Cell Membranes**

4

5 Xiangyang Guo¹, Jan Steinkühler², Mariana Marin¹, Xiang Li³, Wuyuan Lu⁴, Rumiana
6 Dimova² and Gregory B. Melikyan^{1,5#}

7

8 ¹ Department of Pediatrics, Emory University School of Medicine, Atlanta, GA 30322,
9 United States;

10 ² Max Planck Institute of Colloids and Interfaces, 14424 Potsdam, Germany;

11 ³ School of Pharmacy, Second Military Medical University, Shanghai, 200433, China;

12 ⁴ Institute of Human Virology and Department of Biochemistry and Molecular Biology,
13 University of Maryland School of Medicine, Baltimore, Maryland 21201, United States;

14 ⁵ Children's Healthcare of Atlanta, Atlanta, GA 30322, USA.

15

16 # Corresponding author: Gregory B. Melikyan, gmeliki@emory.edu

17

18 **Abstract**

19 Interferon-induced transmembrane protein 3 (IFITM3) potently inhibits entry of
20 diverse enveloped viruses by trapping the viral fusion at a hemifusion stage, but the
21 underlying mechanism remains unclear. Here, we show that recombinant IFITM3
22 reconstituted into lipid vesicles induces negative membrane curvature and that this
23 effect maps to its small amphipathic helix (AH). We demonstrate that AH: (i) partitions
24 into lipid-disordered domains where IAV fusion occurs, (ii) induces negative
25 membrane curvature, and (iii) increases lipid order and membrane stiffness.
26 Additionally, replacing the IFITM3 AH with AH from an unrelated protein did not
27 compromise its antiviral activity. These effects on membrane properties correlate with
28 the fusion-inhibitory activity, as exogenous addition of AH to insulin-producing cells
29 reduces glucose-stimulated insulin secretion. Our results thus imply that IFITM3
30 inhibits the transition from hemifusion to full fusion by imposing an unfavorable
31 membrane curvature and increasing the order and stiffness of the cytoplasmic leaflet of
32 endosomal membranes.

33

34

35

36 Key words: IFITM3; viral fusion; hemifusion; amphipathic helix; membrane curvature;
37 membrane rigidity

38

39 **Introduction**

40 Infection by enveloped viruses proceeds through fusion of the viral membrane with the
41 target cell membrane. Viral fusion, which is a critical step for establishing infection, is
42 mediated by viral fusion proteins that are transmembrane glycoproteins protruding
43 from the virus envelope. When activated by binding to cellular receptors and/or by
44 acidic pH in endosomes, viral fusion proteins undergo extensive conformational
45 changes (Harrison, 2008). As a result of this refolding, the two contacting membrane
46 leaflets merge to form a hemifusion diaphragm (Chernomordik & Kozlov, 2003), which
47 allows lipid mixing between the contacting leaflets, and ultimately culminates in full
48 fusion through the formation of a fusion pore. Finally, enlargement of a fusion pore
49 allows the release of the viral content into the cytosol and initiates infection.

50
51 Interferon-induced transmembrane proteins (IFITMs) are host factors that broadly and
52 potently inhibit infection of diverse enveloped viruses, including the Influenza A virus
53 (IAV), Dengue virus, Severe Acute Respiratory Syndrome-associated coronavirus
54 (SARS-CoV), Respiratory Syncytial Virus (RSV) and Ebola virus (EBOV) (Brass et
55 al., 2009; Diamond & Farzan, 2013). The IFITM family includes IFITM1 that localizes
56 predominantly at the plasma membrane (Huang et al., 2011; Mudhasani et al., 2013),
57 as well as IFITM2 and IFITM3, which contain an endocytic signal in their cytoplasmic
58 N-terminal domain and are predominantly found in late endosomes and lysosomes
59 (Amini-Bavil-Olyaei et al., 2013; Feeley et al., 2011). IFITM3 alone is responsible for
60 the bulk of antiviral effects of interferon in cell culture (Brass et al., 2009) and has been
61 shown to be important for restricting viral replication in cell culture and *in vivo* (Bailey,
62 Huang, Kam, & Farzan, 2012; Everitt et al., 2013; Everitt et al., 2012; Y. H. Zhang et
63 al., 2013).

64
65 While the importance of IFITM3 in host antiviral defenses *in vitro* and *in vivo* is well-
66 documented, its mechanism of action is not clearly defined. IFITMs are type II
67 transmembrane proteins with a cytoplasmic N-terminus, followed by a hydrophobic
68 membrane-associated region and a C-terminal transmembrane domain (Bailey, Kondur,
69 Huang, & Farzan, 2013; Ling et al., 2016). A number of residues scattered across the
70 cytoplasmic region of IFITM3 have been shown to be essential for antiviral activity

71 (John et al., 2013). The most popular view of the mechanism of IFITM3's antiviral
72 activity is that IFITM3 creates "tough membranes" that are not conducive to fusion,
73 most likely by altering membrane curvature and fluidity (Chesarino et al., 2017; John
74 et al., 2013; Li et al., 2013; Lin et al., 2013), but direct evidences and detailed
75 mechanisms are lacking. Using single virus tracking in live cells, we have previously
76 discovered that IFITM3 traps the IAV at a "dead-end" hemifusion stage that does not
77 culminate in full fusion (Desai et al., 2014). In other words, IFITM3 does not restrict
78 the lipid-mixing stage of viral fusion, but rather inhibits the formation of a fusion pore.

79

80 There is evidence suggesting that IFITMs may inhibit viral fusion *via* an indirect
81 mechanism that involves recruitment or modulation of other host factors. First, IFITM3
82 has been reported to bind to and inhibit the function of vesicle-associated membrane
83 protein-associated protein A (VAPA) (Amini-Bavil-Olyaei et al., 2013), which
84 disrupts cholesterol transport from late endosomes and causes its accumulation in these
85 compartments. However, high cholesterol content itself does not appear to inhibit virus-
86 endosome fusion (Desai et al., 2014; Lin et al., 2013; Wrensch, Winkler, & Pohlmann,
87 2014; Wu et al., 2020). Second, it has been proposed that IFITM3 works by recruiting
88 zinc metalloprotease ZMPSTE24 to endosomes and that this effector protein is
89 responsible for virus restriction (Fu, Wang, Li, & Dorf, 2017). However, several lines
90 of evidence support a direct mechanism of IFITM3-mediated virus restriction. We have
91 employed single virus tracking in live cells expressing a functional IFITM3 protein
92 tagged with autofluorescent proteins and shown that IAV enters IFITM3-enriched
93 endosomes where it undergoes hemifusion, but fails to complete the fusion process
94 (Suddala et al., 2019). We found that, by contrast, the IFITM3-resistant Lassa virus
95 enters through a distinct pathway that utilizes endosomes devoid of IFITM3. Moreover,
96 IFITM3 incorporation into the viral membrane inhibits fusion mediated by both
97 IFITM3-sensitive and -resistant viral glycoproteins (Suddala et al., 2019; Tartour et al.,
98 2017). These results suggest that IFITM3 inhibits viral fusion by a proximity-based
99 mechanism that requires the presence of this factor at the sites of viral fusion.

100

101 Here, using liposome-based *in vitro* reconstitution assays, we provide evidence that
102 IFITM3 restricts membrane fusion by inducing unfavorable negative curvature and

103 stiffening the cytoplasmic leaflet of a target membrane at the site of viral hemifusion
104 and that these effects map to the small amphipathic helix region of IFITM3.

105 **Results**

106 **IFITM3 induces negative membrane curvature *in vitro***

107 To understand the molecular mechanism by which IFITM3 inhibits viral fusion, we
108 sought to purify recombinantly expressed IFITM3 and its derivatives, reconstitute these
109 into liposomes and assess their effects on the properties of lipid bilayers. For the
110 purification purposes, we tagged IFITM3 with an N-terminal Strep-tag (Figure 1A) and
111 verified its antiviral activity by expressing it in HEK 293T cells (Fig. S1A) and testing
112 its ability to inhibit the influenza A virus (IAV) infection (Figure S1B). Next, the tagged
113 IFITM3 was expressed in *Escherichia coli*, extracted by Triton X-100 and purified
114 (Figure 1B). In order to visualize the IFITM3 association with membranes, we
115 expressed and purified a fluorescently-tagged IFITM3 (referred to as IFITM3-iEGFP,
116 Fig. 1A), with EGFP inserted into the N-terminal region of the protein (Suddala et al.,
117 2019). We have previously shown that EGFP insertion does not compromise the
118 antiviral activity of IFITM3 (Suddala et al., 2019). The purified proteins were then
119 incorporated into preformed large unilamellar vesicles (LUVs) made of 16:0-18:1
120 phosphatidylcholine (POPC) and cholesterol, using a detergent-mediated reconstitution
121 protocol (Rigaud & Levy, 2003). Here, detergent removal from a lipid/protein mixture
122 through hydrophobic adsorption onto Bio-Beads SM-2 triggers protein insertion into
123 lipid bilayers to generate proteoliposomes. Density gradient LUV flotation showed that
124 both IFITM3 and IFITM3-iEGFP were efficiently incorporated into the liposomes
125 (Figure S1C).

126 We next tested the sidedness of IFITM3 incorporation based upon its accessibility to
127 proteolysis by trypsin. Addition of trypsin to IFITM3- or IFITM3-iEGFP-reconstituted
128 liposomes resulted in a nearly complete cleavage of both molecules, similar to cleavage
129 following proteoliposome solubilization in a detergent (Figure S1D). Thus, both
130 reconstituted proteins appear to insert into liposomes in a preferential orientation, with
131 their large cytoplasmic domains exposed to external medium. This result supports

132 proper reconstitution of IFITM3 proteins in liposomes with an orientation similar to
133 that in endosomal membranes (Bailey et al., 2013; Ling et al., 2016) (Fig. 1A).

134 In order to assess whether IFITM3 possesses membrane remodeling activity, IFITM3-
135 or IFITM3-iEGFP-reconstituted proteoliposomes were dehydrated and electroformed
136 into giant unilamellar vesicles (GUVs) using a previously described method (Girard et
137 al., 2004). After formation, the N-terminally strep-tagged IFITM3 reconstituted into
138 GUVs could be visualized by staining with the AlexaFlour-647 labeled streptavidin,
139 further supporting its preferential orientation in lipid bilayers (Figure S1E). Importantly,
140 we consistently observed that, in contrast to control GUVs, vesicles containing either
141 IFITM3 or IFITM3-iEGFP protein contained intraluminal vesicles (ILVs) formed
142 through inward budding of the GUV membrane (Figures 1D and S1E). The formation
143 of ILVs or tubes from GUVs is a direct visualization of preferred or spontaneous
144 membrane curvature (Karimi et al., 2018; Steinkuhler et al., 2020). This important
145 finding implies that IFITM3 is capable of inducing negative membrane curvature, i.e.
146 promoting membrane bending away from the protein (McMahon & Gallop, 2005).

147 We next asked whether the induction of negative membrane curvature by IFITM3 is
148 mediated by its cytosolic domain (residues 1-108) (John et al., 2013; Ling et al., 2016).
149 We therefore constructed a soluble IFITM3 fragment with GFP inserted into its N-
150 terminal region (designated IFITM3(1-108)-iEGFP, Fig. 1A) and purified it without
151 detergent solubilization (Figure 1C). Interestingly, IFITM3(1-108)-iEGFP showed
152 very weak membrane binding to LUVs (<5% of protein input), as assessed by a
153 liposome co-sedimentation assay (Julkowska, Rankenberg, & Testerink, 2013) (Figure
154 S1F). Next, purified IFITM3(1-108)-iEGFP was added to preformed GUVs containing
155 POPC and cholesterol prepared using a standard electroformation method (Angelova
156 & Dimitrov, 1986). IFITM3(1-108)-iEGFP but not EGFP protein induced inward
157 budding and formation of ILVs within 20 minutes of addition to GUVs, as illustrated
158 by time-resolved imaging (Fig. 1E). As expected, intraluminal vesicles trapped
159 IFITM3(1-108)-iEGFP from external solution (Figure 1E). Quantification of the
160 inward budding effect of this protein showed that 75% of GUVs treated with IFITM3(1-
161 108)-iEGFP contained ILVs and each GUV contained, on average, 1.7 ILVs (Figure
162 1F, G). By contrast, EGFP-treated GUVs rarely contained ILVs and any ILVs detected

163 were not filled with EGFP, suggesting that these structures formed during GUVs
164 electroformation. These results imply that the IFITM3 cytosolic domain induces
165 negative membrane curvature, in spite of poor binding to membranes, and that the
166 transmembrane domain is dispensable for this activity.

167 **IFITM3 amphipathic helix is responsible for induction of negative membrane**
168 **curvature**

169 It has been shown that a highly conserved small region (residues 59-68) of the
170 IFITM3's cytoplasmic domain, predicted to form an amphipathic helix (AH), is
171 essential for antiviral activity (Chesarino et al., 2017; Z. Zhang, Liu, Li, Yang, & Zhang,
172 2012). Since many amphipathic helices can sense membrane curvature or induce
173 membrane remodeling (Drin & Antony, 2010), we asked whether the AH of IFITM3
174 is responsible for its ability to induce negative membrane curvature. To answer this
175 question, we made a triple alanine substitutions S61A, N64A, T65A (designated
176 IFITM3-3M, Figure 2A) in the AH region, which have been shown to greatly reduce
177 the amphipathic moment of the AH and abrogate the antiviral activity against IAV (Fig.
178 2A) (Chesarino et al., 2017). The IFITM3-3M mutant was purified (Figure S2A) and
179 reconstituted into GUVs (Figure 2B). We found that the inward budding activity of the
180 GUV-reconstituted IFITM3-3M was significantly impaired compared to wild-type
181 IFITMs. Only 7.1% of IFITM3-3M-reconstituted GUVs contained at least one ILV, as
182 compared 81.7% of wild-type IFITM3-reconstituted GUVs (Figure 2B, C). We also
183 tested the triple alanine mutant in the context of the IFITM3 cytosolic domain tagged
184 with EGFP (IFITM3(1-108)-3M-iEGFP) and found that this soluble construct also
185 exhibited impaired ILV-forming activity when added to preformed GUVs (Figure S2B-
186 E). The above results map the negative curvature-promoting activity of IFITM3 to its
187 AH.

188

189 To determine whether IFITM3 AH alone is sufficient to induce negative membrane
190 curvature, a peptide corresponding to this region (residues 59-68) and a longer peptide
191 (residues 56-71) were synthesized and labeled with Cy-5 dye at their N terminus
192 (Figure 2A). A peptide with scrambled amino acid sequence (Scrambled AH(56-71))
193 and the F63Q AH(59-68) mutant peptide (AH(59-68) F63Q) were used as controls.

194 Substitution of the hydrophobic F63 residue to glutamine has been shown to markedly
195 decrease the peptide's amphipathicity (Fig. 2A) and nearly abrogate its antiviral activity
196 (Chesarino et al., 2017). The partition coefficients of the peptides, which reflect their
197 membrane binding affinity, were measured using a liposome co-sedimentation assay
198 (Figure S2F). The AH(56-71), AH(59-68) and Scrambled AH(56-71) peptides
199 exhibited similar membrane binding affinities, with more than 80% of the input peptide
200 binding to liposomes (at input peptide to lipid ratio 1:50). The AH(59-68) F63Q
201 exhibited a slightly weaker membrane binding affinity, with 58.4% of the input peptide
202 binding to liposomes.

203

204 Next, membrane binding and remodeling activity of these peptides added to GUVs
205 were tested by imaging. All peptides were clearly enriched at the GUV membrane
206 (Figure 2D), consistent with the membrane partitioning data (Fig. S2F). Strikingly,
207 addition of AH(56-71) or AH(59-68) peptides to preformed GUVs containing POPC
208 and cholesterol led to efficient inward budding, resulting in 68.5% and 74.7% of the
209 GUVs containing at least one ILV, respectively (Figure 2D, E). These inner vesicles
210 contained the aqueous marker fluorescein, which was added to GUVs externally, along
211 with the peptides, in order to ensure that ILVs were formed *de novo* through inward
212 budding (Figure 2D). Importantly, addition of the same concentration of the Scrambled
213 AH(56-71) peptide or a 2-fold excess of the AH(59-68) F63Q peptide (to compensate
214 for its slightly lower membrane affinity) did not induce considerable GUV vesiculation,
215 with respectively 9.9% and 16.6% of the GUVs containing ILVs (Figure 2D, E). ILVs
216 seemed to fission from the outer membrane as judged by their position in the GUVs,
217 which is consistent with a recent finding of membrane fission of buds due to high
218 membrane spontaneous curvature (Steinkuhler et al., 2020). Taken together, these
219 results confirmed that IFITM3 AH alone is sufficient to induce negative membrane
220 curvature and that this effect is critically dependent on the amphipathicity of this region.

221 **Negative membrane curvature induced by IFITM3 is facilitated by cholesterol** 222 **and counteracted by lyso-lipids**

223 Different lipids have different effective shapes manifested in spontaneous curvature
224 that can impose positive or negative curvature to a lipid bilayer (Helfrich, 1973). Thus,

225 biological membrane curvature is determined by an interplay between membrane
226 proteins and lipids (Bassereau et al., 2018; Stachowiak, Hayden, & Sasaki, 2010;
227 Steinkuhler et al., 2020). Lipids are categorized as “cylindrical”, “cone”, and “inverted
228 cone” shaped. Cylindrical lipids, such as phosphatidylcholine (PC), prefer planar
229 membranes, whereas cone-shaped lipids, such as cholesterol and
230 phosphatidylethanolamine (PE), prefer negative membrane curvature, and inverted
231 cone-shaped lipids, like Lyso-PC (LPC), promote positive membrane curvature
232 (Kozlov, 2007).

233 We therefore tested whether lipids play a role in IFITM3-mediated GUV vesiculation.
234 First, we electroformed POPC GUVs with or without cholesterol (0.5 mol%) and
235 treated these with IFITM3(1-108)-iEGFP. Whereas this treatment resulted in 75.5% of
236 cholesterol-containing GUVs with ILVs, a significant impairment of inward budding
237 (8.5% GUVs with ILVs) was observed in the absence of cholesterol (Figure 3A, B).
238 Similarly, addition of the AH(56-71) peptide to GUVs without cholesterol also failed
239 to induce efficient inward budding (Figure S3A, B). Notably, IFITM3-induced inward
240 budding in GUVs was independent of cholesterol concentration up to 20 mol% (Figure
241 S3C). Importantly, AH(56-71) mediated inward budding of GUVs without cholesterol
242 could be rescued by inclusion of another conical lipid, DOPE (20 mol%) (Figure S3D).
243 This finding indicates that IFITM3-induced negative membrane curvature is facilitated
244 by cone shaped lipids.

245 We next tested the effect of a conical lipid, LPC, on GUV budding mediated by IFITM3.
246 LPC was first titrated by adding to preformed GUVs containing POPC and cholesterol.
247 As expected based upon positive curvature induced by this lipid (Fuller & Rand, 2001),
248 we observed outward budding of the GUV membrane in an LPC dose-dependent
249 manner (Figure S3E). A moderate concentration of LPC (10 μ M) was then added
250 together with the AH(56-71) peptide to preformed GUVs containing POPC and
251 cholesterol. LPC abolished the AH(56-71)-induced GUV inward budding ([Figure 3C,](#)
252 [D](#)), showing that negative membrane curvature caused by IFITM3 is counteracted by
253 the presence of conical lipid in the membrane.

254 **IFITM3 partitions into liquid-disordered membrane domains that support IAV**
255 **fusion**

256 Cell membranes contain lipid rafts, which are liquid-ordered domains with more tightly
257 packed lipids than the non-raft, liquid-disordered phase of the bilayer (Rajendran &
258 Simons, 2005a). Lipid rafts form a platform for signaling proteins and receptors and
259 have been suggested to serve as potential virus entry sites (Chazal & Gerlier, 2003), but
260 a formal proof is still lacking due to the fact that small and dynamic lipid microdomains
261 are difficult to visualize in living cells. Post-translational modifications, such as S-
262 palmitoylation, target transmembrane proteins to lipid rafts (Levental, Lingwood,
263 Grzybek, Coskun, & Simons, 2010). Palmitoylation of the conserved cysteine residues
264 downstream of the IFITM3 AH region regulate the membrane domain targeting and
265 antiviral activity of this protein (Yount et al., 2010). We therefore asked whether
266 IFITM3 has any preference to lipid microdomains and whether lipid rafts may play a
267 role in IFITM3's antiviral activity. To address this question, we utilized phase-
268 separated GUVs as a model for microdomains within the endosomal membrane (Kaiser
269 et al., 2009). GUVs containing sphingomyelin (SM), cholesterol and poly-unsaturated
270 phosphatidylcholine (DOPC) segregate into lipid ordered (Lo) and lipid disordered (Ld)
271 phases (Wesolowska, Michalak, Maniewska, & Hendrich, 2009) corresponding to lipid
272 raft and non-raft microdomains of biological membranes, respectively. Incorporation
273 of fluorescent markers partitioning into Lo (Top-cholesterol) or Ld (Liss-Rho-PE)
274 phases allowed the visualization of the two phases (Figure 4A, B). The AH(56-71)
275 peptide added to phase-separated GUVs partitioned to the Ld phase and caused inward
276 budding from this domain, as evidenced by ILVs containing exclusively the Ld marker
277 Liss-Rho-PE (Figure 4C). The Scrambled AH(56-71) peptide also exhibited an Ld
278 phase preference, but failed to cause inward budding from this phase (Figure 4C).
279 Intriguingly, palmitoylation of Cys71 of a fluorescently-tagged AH(56-75) peptide did
280 not target this peptide to Lo phase. This peptide clearly partitioned to the Ld phase and
281 appeared to concentrate at the phase boundary (Figure S4A).

282 We then asked whether the full-length IFITM3 protein similarly localizes to the Ld
283 phase in cellular membranes. IFITM3 transits through the plasma membrane *en route*
284 to endolysosomal compartments and is thus present on the cell surface (Jia et al., 2014).

285 We thus used plasma membrane-derived spheres (Lingwood, Ries, Schwille, & Simons,
286 2008) to visualize IFITM3 partitioning into membrane rafts. We expressed IFITM3
287 with an internal SNAP-tag inserted at the same site as EGFP in IFITM3-iGFP (Suddala
288 et al., 2019). SNAP-tagged IFITM3 was expressed in A549 cells and specifically
289 labeled with a fluorescent substrate SNAP-Cell 647-SiR. Next, membrane spheres
290 derived from the plasma membrane were obtained by cell swelling and phase separation
291 within these spheres was induced by crosslinking a lipid raft marker GM1 with a labeled
292 cholera toxin B subunit (Lingwood et al., 2008) (Figure 4D). The IFITM3-iSNAP
293 partitioned to the Ld phase of membrane spheres, suggesting that the full-length
294 IFITM3 is also localized to non-raft domains in living cells (Figure 4D).

295 Next, we sought to test whether the IFITM3 localization to Ld phase may be augmented
296 for its antiviral activity. To answer this question, we employed a lipid mixing assay
297 between IAV labeled with a self-quenching concentration of the lipophilic dye DiD and
298 GUVs. Here, addition of labeled IAV to GUVs followed by acidification should trigger
299 lipid mixing which can be detected by the appearance of dequenched DiD in the GUV
300 membrane (Figure 4E). Using phase-separated GUVs, we found that, upon triggering
301 IAV-GUV fusion by exposure to low pH, DiD accumulated within the Ld domain
302 (Figure S4B), although in the presence of IAV receptor ganglioside GM1, which
303 dominantly accumulates in Lo domain (Figure S4C), suggesting that IAV lipid mixing
304 occurred in a non-raft phase ~~(Figure S4C)~~. To test the possibility of DiD redistribution
305 between Lo and Ld phases after viral fusion, single-phase GUVs were prepared. Low
306 pH-induced IAV lipid mixing occurred very efficiently with Ld-phase GUVs (Figure
307 4F), whereas no lipid mixing was detected between IAV and Lo-phase GUVs, in spite
308 of the efficient binding of labeled viruses to these vesicles (Figure 4F). Taken together,
309 these results imply that IFITM3 concentrates in non-raft domains which appear to be
310 the sites supporting IAV fusion in synthetic membranes.

311 **IFITM3 amphipathic helix increases lipid order and stiffens membranes**

312 Since IFITM3 tends to localize to non-raft microdomains of membranes and induces
313 negative curvature through its AH, we asked whether this helical domain affects other
314 membrane properties, such as lipid order and membrane stiffness. Lipid order, which

315 reflects the mobility of hydrocarbon tails of lipids (Vanblitterswijk, Vanhoeven, &
316 Vandermeer, 1981), has been assessed using the lipophilic probe Laurdan. Laurdan is
317 an environment-sensitive dye that intercalates between the hydrocarbon tails of lipids
318 and exhibits a red-shift in the emission spectrum upon exposure to polar solvent, i.e.,
319 in lipid disordered domains. The Laurdan emission shift is parameterized by
320 generalized polarization (GP), which is a normalized difference between Laurdan's
321 emission at two wavelengths (Parasassi, De Stasio, Dubaldo, & Gratton, 1990) (Figure
322 5A). We thus used Laurdan to probe the effect of IFITM3 AH peptides on LUVs.
323 Addition of either AH(56-71) or AH(59-68) peptide caused a strong positive shift in
324 the Laurdan GP, indicating a marked increase in lipid order (Figure 5B). In contrast,
325 the AH(59-68) F63Q mutant did not have a significant effect on GP, and the Scrambled
326 AH(56-71) peptide only modestly altered GP. A detectable effect of the scrambled
327 peptide on GP is likely due to its higher binding affinity to membranes (Figure 5B).
328 These findings imply that IFITM3 AH specifically increases the lipid order.

329 It has been reported that lipid order correlates with the bending rigidity of cellular
330 membranes (Steinkuhler, Sezgin, Urbancic, Eggeling, & Dimova, 2019). We therefore
331 asked whether IFITM3 AH can affect the membrane's bending rigidity. The membrane
332 bending rigidity was measured by fluctuation analysis of the thermally induced motion
333 of GUV membrane, as described previously (Gracia, Bezlyepkina, Knorr, Lipowsky,
334 & Dimova, 2010). Addition of AH(56-71) resulted in significant increase in the bending
335 rigidity of the GUV membrane (Figure 5C). In contrast, the Scrambled AH(56-71)
336 peptide did not have a significant effect on the bending rigidity. These important
337 findings show that IFITM3 AH specifically stiffens lipid membranes and increases the
338 lipid order.

339 **IFITM3 amphipathic helix alone is sufficient to inhibit membrane fusion**

340 The ability of IFITM3 AH to induce negative curvature, increase the lipid order and
341 stiffen the membrane implies that region is responsible for the protein's inhibitory
342 effect on viral fusion. We hypothesized that AH interaction with the cytoplasmic leaflet
343 of endosomal membranes is necessary and sufficient for the antiviral activity IFITM3.
344 However, testing this hypothesis *in vitro* using reconstituted IFITM3 peptides is not

345 feasible. This is because incoming viruses do not come into contact with the N-terminal
346 cytoplasmic region of IFITM3 that encompasses the AH, whereas reconstituted
347 IFITM3 and IFITM3 AH localize to the external leaflet of endosomes (Figure 1A) that
348 comes in contact with exogenously added viruses. To fulfill the topological requirement
349 for virus/IFITM3 positioning across a target membrane, using exogenously added
350 peptides, we resorted to exocytosis (Figure 6A). Secretory vesicle fusion with the
351 plasma membrane affords an easy access to the external (trans) leaflet of a target
352 membrane. We used glucose-stimulated insulin secretion as a model to study the effect
353 of IFITM3 on SNARE-mediated vesicle fusion (Figure 6A). INS-1E cells secrete
354 insulin upon stimulation with high glucose (Merglen et al., 2004). To increase the
355 sensitivity of detection of secreted insulin, INS-1E cells were transduced with a vector
356 expressing a proinsulin-luciferase fusion protein (Burns et al., 2015), which can be
357 detected by luciferase activity following exposure to a high glucose solution (Figure
358 6B). When cells were pretreated with AH(59-68), which effectively bound to the
359 plasma membrane (Figure S5A), high glucose stimulation resulted in significantly
360 reduced insulin secretion. In contrast, the AH(59-68) F63Q peptide had no effect on
361 insulin secretion, even when added in a higher concentration than the wild-type peptide
362 (Figure 6B, Figure S5B). To test whether inhibition of secretion was related to the
363 IFITM3 AH-mediated negative membrane curvature, we pretreated cells with LPC,
364 which induces positive curvature. LPC promoted insulin secretion, in agreement with
365 the previous study (Amatore et al., 2006) (Figure 6C). Importantly, LPC added with
366 IFITM3 AH counteracted the suppression of insulin secretion by this peptide. Taken
367 together, these results imply that IFITM3 AH is sufficient to inhibit membrane fusion
368 and that this inhibition is dependent on its ability to induce negative membrane
369 curvature.

370

371 To further investigate the link between membrane curvature and antiviral activity of
372 IFITM3, we asked whether the IFITM3 AH can be replaced with unrelated amphipathic
373 helices of other proteins, such as M2 of IAV (M2 AH). The M2 AH has been reported
374 to induce negative curvature and increase lipid order during IAV budding from the
375 plasma membrane (Martyna et al., 2017; Rossman, Jing, Leser, & Lamb, 2010). We
376 thus replaced the IFITM3 AH with M2 AH in the context of an mTFP1 tagged protein

377 (abbreviated IFITM3-M2 AH-imTFP1, Figure 7A). We also constructed a scrambled
378 IFITM3 AH mutant (IFITM3-Scrambled AH-imTFP1) as a control (Figure 7A). When
379 overexpressed in HEK 293/17 cells, wild-type IFITM3 significantly inhibited the
380 infection of the mCherry-expressing IAV (Figure 7B, C). As expected, the scrambled
381 IFITM3 AH mutant exhibited a markedly attenuated antiviral activity against IAV.
382 Importantly, IFITM3 chimera with the M2 AH showed strong antiviral activity, without
383 significantly affecting cell viability (Figure S5C). The demonstration that IFITM3 AH
384 can be replaced by other negative curvature-inducing and lipid-ordering AHs further
385 confirms that IFITM3 inhibits viral fusion by modulating the properties of endosomal
386 membrane through its amphipathic helix.
387

388 **Discussion**

389 A remarkably broad-spectrum of enveloped viruses that are restricted by IFITM
390 proteins suggests a universal mechanism for their antiviral activity. This mechanism
391 may involve modifying the properties of the host cell membranes to disfavor fusion
392 pore formation and thus trap viral fusion at a “dead-end” hemifusion stage (Desai et al.,
393 2014; Suddala et al., 2019). Here, we provided direct evidence for this mechanism by
394 showing that lipid bilayer-reconstituted recombinant IFITM3 induces unfavorable
395 negative curvature and increases the lipid order and membrane stiffness. Importantly,
396 we found that these effects on lipid bilayers *in vitro* are linked to the IFITM3’s ability
397 to inhibit membrane fusion in cells. Specifically, we showed that the incorporation of
398 IFITM3 AH into the external leaflet of the plasma membrane inhibits exocytosis
399 (Figure 6B). Although exocytic fusion is the topological opposite of viral fusion, it
400 provides a convenient model system for assessing the effects of exogenously added
401 amphipathic peptides and lipids (Amatore et al., 2006; Burns et al., 2015).

402 According to the stalk-pore hypothesis (Chernomordik, Melikyan, & Chizmadzhev,
403 1987; Kozlov, Leikin, Chernomordik, Markin, & Chizmadzhev, 1989), membrane
404 fusion proceeds through a series of highly curved intermediates – stalk, hemifusion and
405 fusion pore – that are characterized by different net curvatures and thus respond
406 differently to changes in lipid shape/composition. The formation of a lipid stalk

407 involves a local disruption and bending of contacting membrane leaflets into a net
408 negative curvature structure (Figure 7D). The hemifusion intermediate is also a net
409 negative curvature structure, whereas the fusion pore possesses a net positive curvature
410 (Figure 7D) (Chernomordik & Kozlov, 2003). Thus, the presence of lipids that induce
411 positive curvature, such as LPC, in the contacting leaflets blocks the stalk formation,
412 whereas their incorporation into the distal leaflet of a target membrane, promotes
413 rupture of the hemifusion diaphragm and fusion pore formation (Amatore et al., 2006;
414 Chernomordik, Frolov, Leikina, Bronk, & Zimmerberg, 1998; Chernomordik et al.,
415 1987; Stiasny & Heinz, 2004). In contrast, fusion pore formation is impaired by lipids
416 inducing negative curvature, such as oleic acid (OA) (Chernomordik, Leikina, Frolov,
417 Bronk, & Zimmerberg, 1997). Thus, spontaneous curvature of lipids is an essential
418 determinant of membrane hemifusion and fusion mediated by cellular and viral proteins
419 (Chernomordik & Kozlov, 2003).

420 Our experiments demonstrate that, similar to OA, IFITM3 AH induces negative
421 curvature of GUVs manifested in inward budding and ILV formation. Thus, in the
422 context of IFITM3 expressed in cells, AH inserted into the cytoplasmic leaflet of an
423 endosomal membrane is expected to stabilize the hemifusion diaphragm formed by
424 incoming viruses and thus prevent the fusion pore formation (Figure 7D). In addition,
425 the increased membrane order and stiffness induced by IFITM3 are expected to further
426 disfavor membrane fusion (Chesarino et al., 2017; John et al., 2013; Li et al., 2013; Lin
427 et al., 2013).

428 Our finding that IFITM3 induces negative curvature and inward budding in GUVs is
429 consistent with the observation that its overexpression in cells robustly induced the
430 formation of large multivesicular bodies that are full of IFITM3-containing
431 intraluminal vesicles (Amini-Bavil-Olyaei et al., 2013). These results also support the
432 “fusion decoy” model, according to which excess of intraluminal vesicles in IFITM3-
433 expressing cells favors non-productive viral fusion with intraluminal vesicles, instead
434 of fusion with the limiting membrane of endosomes (Desai et al., 2014). The above
435 considerations suggest that a potent inhibition of diverse enveloped viruses by IFITM3
436 may involve a combination of modulation of membrane properties and generation of
437 an excess of decoy vesicles in endosomes.

438 Lipid raft domains have been proposed to be the entry sites of viruses due to the raft
439 localization of certain signaling proteins and receptors (Chazal & Gerlier, 2003).
440 However, direct evidence supporting this model is lacking due, in part, to the dynamic
441 nature of raft micro- and nano-domains in living cells (Rajendran & Simons, 2005b).
442 In addition, the rigid nature of lipid raft domains is expected to disfavor membrane
443 fusion. Interestingly, it has been reported that the boundaries between ordered and
444 disordered lipid domains, which are characterized by high line tension (energy per unit
445 length), are the predominant sites of HIV-1 fusion (Yang et al., 2017). However, such
446 apparent preference for domain boundaries is not universal, since IAV lipid mixing
447 occurs efficiently with Ld-phased GUVs lacking lipid rafts or phase boundaries (Figure
448 4F). No lipid mixing could be detected with Lo GUVs. A correlation between the
449 apparent IAV fusion site and the IFITM3 localization to Ld phase may offer a clue
450 regarding the potential mechanism of virus resistance. It is tempting to speculate that
451 IFITM3-resistant viruses, like Lassa virus, may localize to and fuse with lipid raft
452 domains devoid of this restriction factor.

453 It is worth pointing out that AH is present in IFITM1 and IFITM2 proteins and is highly
454 conserved across vertebrates (Chesarino et al., 2017; Z. Zhang et al., 2012). It is
455 therefore very likely that the AH region is key to the antiviral activity of all three human
456 restriction factors. Clearly, this novel proximity-based antiviral mechanism is
457 dependent on proper trafficking of IFITMs to ensure their concentration at the sites of
458 virus entry (Li et al., 2013; Suddala et al., 2019). Accordingly, incorporation of IFITMs
459 into virions ensures their presence at the site of fusion and effectively inhibits infection
460 of nearly all viruses, including those that are otherwise resistant to IFITM restriction
461 when expressed in target cells (Appourchaux et al., 2019; Suddala et al., 2019; Tartour
462 et al., 2017)

463 Our findings reveal a universal defense mechanism employed by cells to effectively
464 ward off invading enveloped viruses through modification of the cytoplasmic leaflet of
465 cellular membranes. The IFITM AH-mediated increases in negative curvature and
466 stiffness of the cytoplasmic leaflet disfavor the transition from hemifusion to full fusion
467 and thereby block entry of diverse enveloped viruses. This restriction mechanism

468 informs us of novel antiviral strategies targeting the cytoplasmic leaflet of cell
469 membranes.

470 **Materials and Methods**

471

472 **Cell lines, plasmids and reagents**

473 HEK293T/17 and A549 cells were obtained from ATCC (Manassas, VA) and were
474 maintained in Dulbecco's Modified Eagle Medium (DMEM, Corning, Corning, NY)
475 containing 10% heat-inactivated Fetal Bovine Serum (FBS, Atlanta Biologicals,
476 Flowery Branch, GA) and 1% penicillin/streptomycin (Gemini Bio-products, West
477 Sacramento, CA). For HEK 293T/17 cells, the growth medium was supplemented with
478 0.5 mg/ml G418 (Genesee Scientific, San Diego, CA). INS-1E cells were obtained from
479 Addexbio Technologies (San Diego, CA, USA) and were maintained in RPMI-1640
480 Medium (Addexbio), supplemented with 10% heat-inactivated FBS, 10 mM HEPES,
481 and 55 μ M β -mercaptoethanol (Invitrogen, Carlsbad, CA). pET28a vector was a gift
482 from Dr. Baek Kim (Emory University). pQCXIP was purchased from Clontech
483 (Mountain View, CA). Proinsulin-NanoLuc in pLX304 vector (plasmid # 62057),
484 psPAX2 packaging plasmid (plasmid #12260) and pMD2.G envelope plasmid (plasmid
485 #12259) were from Addgene (Watertown, MA). N-terminally Cy5-labeled peptides
486 were synthesized and purified to > 95% purity by Gen-Script (Piscataway, NJ). Peptide
487 sequences used were: wt-long, Cy5-DHVVWSLFNTLFMNPC; scrambled peptide,
488 Cy5-LVWHMFLSDNFTNPV; wt-short, Cy5-CVWSLFNTLFM and F63Q short,
489 Cy5-CVWSLQNTLFM. The fluorescently labeled, palmitoylated IFTIM3 peptide
490 (FITC-Ahx-DHVVWSLFN TLFMNPC(PAL)CLGF) was chemically synthesized on
491 Rink Amide MBHA resin using Fmoc solid phase peptide synthesis, and Fmoc-
492 Cys(Mmt)-OH and Fmoc-Ahx-OH, among other Fmoc-protected amino acids. After
493 chain assembly, the Fmoc group of the N-terminus was removed and extended by the
494 linker amino acid Ahx, followed by the coupling of fluorescein isothiocyanate (FITC,
495 2 eq.) and DIPEA (2 eq.) in DMF (6 mL) at room temperature overnight. The
496 monomethoxytrityl (Mmt) group was removed with diluted TFA (2%, DCM) and
497 scavengers (10% TIPS), followed by the addition of palmitic anhydride (10 eq.)
498 dissolved in DCM and DIEA (20 eq.) for 3 h. After cleavage from the resin and

499 precipitation with cold diethyl ether, the crude peptide was purified by reversed phase
500 HPLC and its molecular mass verified by ESI-MS.

501 mCherry-expressing IAV PR/8/34 was a gift from Dr. Luis Martinez-Sobrido
502 (University of Rochester). The following lipids were purchased from Avanti Polar
503 Lipids (Alabaster, AL): 1-oleyl-2-palmitoyl-sn-glycero-3 phosphocholine (POPC),
504 1,2-dioleoyl-sn-glycero-3-phosphocholine (DOPC), 1-stearoyl-2-hydroxy-sn-glycero-
505 3-phosphocholine (18:0 Lyso PC), N-stearoyl-D-erythro-sphingosylphosphorylcholine
506 (18:0 SM), 23-(dipyrrometheneboron difluoride)-24-norcholesterol (TopFluor®
507 Cholesterol), cholesterol (plant derived), and 1,2-dioleoyl-sn-glycero-3-
508 phosphoethanolamine-N-(lissamine rhodamine B sulfonyl) (18:1 Liss-Rho-PE).

509

510 **Protein expression and purification**

511 IFITM3 gene was PCR-amplified and cloned into the pET28a vector to produce
512 recombinant proteins fused to Strep-tag II (WSHPQFEK). Point mutations and
513 deletions were introduced by site-directed mutagenesis. The IFITM3 constructs were
514 transformed into Escherichia coli Rosetta™ 2 (DE3) pLysS Singles™ Competent Cells
515 (MilliporeSigma, Burlington, MA) to overexpress the proteins. The bacteria were
516 cultured in Terrific broth medium at 37°C. Protein expression was induced by the
517 addition of 0.3 mM IPTG when OD600 was 1.0 and culture for additional 20 h at 16°C.
518 Cells were harvested after centrifugation at 2,500 ×g for 30 min, resuspended and
519 sonicated in HND buffer (25 mM HEPES, pH 7.4, 150 mM NaCl, 1 mM DTT)
520 supplemented with cComplete EDTA-free Protease Inhibitor Cocktail (Roche, Basel,
521 Switzerland). The lysate was then centrifuged at 4°C in the SW32Ti rotor with a speed
522 of 30,000 rpm for 1 h to pellet the membrane fraction using an Optima L-90K
523 Ultracentrifuge (Beckman Instruments, Brea, CA). The pellet was resuspended in HND
524 buffer and bulk membrane proteins were extracted by adding 2% ANAPOE-X-100
525 (Anatrace, Maumee, OH) and incubating for 1 h at 4°C, followed by a 1 h-
526 centrifugation at 30,000 rpm. The supernatant was loaded on Strep-Tactin resin
527 (QUIGEN, Hilden, Germany), incubated for 3 h at 4°C, and the column was washed
528 twice with 15 ml HND buffer supplemented with 0.1% ANAPOE-X-100. Proteins were
529 eluted by adding 10 ml HND buffer supplemented with 0.1% ANAPOE-X-100 and 2.5
530 mM desthiobiotin and then concentrated using an Amicon Ultra 5,000 MW cutoff filter

531 (Millipore, Billerica, MA). Protein purity was assessed by SDS-PAGE and Coomassie
532 Blue staining. For purification of wild-type and mutant transmembrane-truncated
533 IFITM3, cell lysate was cleared by centrifugation at 4°C with a speed of 18,000 rpm
534 for 45 min after sonication, and the supernatant was directly loaded on Strep-Tactin
535 resin and incubated for 3 h at 4°C, washed and eluted with the buffer used for
536 purification of the full-length IFITM3 except that ANAPOE-X-100 was omitted.

537

538 **Large Unilamellar Vesicles**

539 Lipids (99.0 mol % POPC, 0.5 mol % cholesterol, 0.5 mol % Liss-Rho-PE) were mixed
540 in a glass tube and dried down to a film under a gentle stream of Argon, followed by
541 further drying under a vacuum for 30 min. Next, the lipid film was hydrated and
542 resuspended with HND buffer to a final lipid concentration of 10 mM. Large
543 unilamellar vesicles (LUVs) were formed from the lipid suspension by ten freeze-thaw
544 cycles using liquid nitrogen and room temperature water bath. Uniform-sized LUVs
545 were formed by extruding through polycarbonate filters with 100-nm pore size (Avanti
546 Polar Lipids, Alabaster, AL) 11 times.

547 To reconstitute IFITM3, preformed liposomes and purified IFITM3 (molar protein to
548 lipid ratio, 1:500) were mixed with 0.1% Triton X-100 at an effective detergent to lipid
549 ratio of ~1 and incubated for 1h at 4 °C. Triton X-100 was then removed by adding
550 BioBeads SM-2 absorbent beads (BioRad) at a Bio-Beads/Triton X-100 ratio of 10
551 (wt/wt) in five portions during the course of hour, and incubating overnight after the
552 final addition of beads. Insoluble protein aggregates were pelleted by centrifugation of
553 samples in an Eppendorf microcentrifuge (10 min, 16,000×g).

554

555 **Liposome co-floatation assay**

556 Peptide binding to LUVs was measured by mixing 204 µl proteoliposomes with 600 µl
557 of a 67% sucrose solution, bringing the final sucrose concentration to 50%. The mixture
558 was transferred to a clear polycarbonate ultracentrifuge tube and overlaid with two
559 layers consisting of 10.2 ml of 25% sucrose and 1 ml of 5% sucrose. After
560 centrifugation at 30,000 rpm (4 °C for 3 h) in the SW45Ti rotor (Beckman Instruments),
561 eight 1.5-ml fractions were collected from the top of a gradient. 30 µl aliquots from

562 each fraction were analyzed by Western blotting with IFITM3 antibody (N-term,
563 Abgent, San Diego, CA).

564

565 **Trypsin cleavage assay**

566 To determine the accessibility of LUV-reconstituted peptides, 20 μ l proteoliposomes
567 was incubated with 0.6 μ g trypsin (TPCK-Treated, Sigma-Aldrich) at 37°C for 30 min.
568 Next, 95°C pre-heated SDS sample buffer (50 mM Tris-HCl, pH 6.8, 2% SDS, 10%
569 glycerol, 1% β -mercaptoethanol, 12.5 mM EDTA, 0.02 % bromophenol blue) was
570 added to stop the reaction. The samples were analyzed by SDS-PAGE and stained with
571 Coomassie blue.

572

573 **Liposome co-sedimentation assay**

574 Peptides were sonicated in water bath for 30 min and possible aggregates were removed
575 by spinning down at 20,000 \times g for 5 min. Two mM of LUVs made of 99.0 mol %
576 POPC, 0.5 mol % cholesterol, 0.5 mol % Liss-Rho-PE in PBS were incubated at room
577 temperature with 20 μ M IFITM3(1-108)-iEGFP protein or 40 μ M of Cy5-labeled
578 peptides for 10 min in a 100 μ l reaction volume. The mixture was then diluted with
579 PBS and centrifuged at 30,000 rpm for 30 min at 20 °C. Fluorescence of supernatant
580 was measured on a SpectraMax i3x microplate reader (Molecular Devices, CA, USA).
581 The binding efficiency of proteins/peptides was decided by reduction of EGFP or Cy5
582 fluorescence in supernatant and normalized by comparing with the fluorescence of
583 input samples.

584

585 **Giant Unilamellar Vesicles**

586 GUVs were prepared from a 5 mM solution of lipids in chloroform (99 mol % POPC,
587 0.5 mol % cholesterol and 0.5 mol % of Liss-Rho-PE). Fifty μ l of the lipid solution was
588 spread onto a 10 cm² area of the conductive side of each of two indium-tin oxide (ITO)
589 coated slides (70-100 Ω , Delta Technologies, Stillwater, MN), allowed to evaporate
590 and kept under vacuum for 1 hr. Electroformation chambers were constructed by
591 sandwiching a 1 mm spacer between two lipid-coated slides. Next, the chamber was
592 filled with 0.1 M sucrose, 1 mM HEPES, pH 7.0, and a 10 Hz sine wave voltage (1 V

593 peak-to-peak) was applied across the chamber for 3 h using a function generator. GUVs
594 were gently collected with a pipette and used immediately.

595 To prepare phase-separated GUVs, we used a mixture of 33 mol % DOPC, 33 mol %
596 SM, 33 mol % cholesterol, 0.5% TopFluor-cholesterol, 0.5% Liss-Rho-PE. Lipids were
597 dissolved in 50 μ l chloroform/methanol (9:1) in a glass tube and placed in a preheated
598 block at 60 °C for 1 min after gentle vortexing and centrifugation. The mixture was
599 then immediately deposited and spread over 2 preheated ITO coverslips, and the solvent
600 was evaporated at 60 °C. After ITO coverslips dried out, they were immediately placed
601 into a vacuum chamber for 1h to remove residual solvent. All these steps were done in
602 a timely manner to minimize possible lipid oxidation. GUV electroformation was
603 carried out in 0.1 M sucrose, 2 mM DTT, 1 mM HEPES, pH 7.0 at 60 °C for 4 h.
604 Collected GUVs were cooled to room temperature and used immediately.

605 For imaging of GUVs with IFITM3 peptides, peptides were prepared as 2 mg/ml stock
606 solutions in DMSO. Twenty μ l GUVs were diluted in 30 μ l of a hypertonic buffer
607 containing 160 mM sucrose, 1 mM HEPES, pH 7.0 to slightly deflate GUVs. Next, 2 μ l
608 of peptide diluted with 98 μ l Hank's Balanced Salt Solution (Corning, NY, USA) was
609 added to and mixed with GUVs, yielding the final concentration of peptide of 10 μ M.
610 The mixture of GUVs and peptide was immediately added to an 8-well chambered
611 coverslip pretreated with a BSA solution (2 mg/ml) for 30 min to attach GUVs to the
612 bottom of the chamber. GUVs were allowed to sediment for 10 min before imaging on
613 a Zeiss LSM880 laser scanning confocal microscopes, using a 63x/1.4NA oil-
614 immersion objective. Purified wild-type and mutant transmembrane-truncated IFITM3
615 proteins were imaged the same way except that the final concentration of proteins was
616 20 μ M. Quantification of inward budding of GUVs was performed by counting all
617 GUVs with diameter above 2 μ m, regardless of whether they encompassed intraluminal
618 vesicles containing aqueous dye (fluorescein or EGFP). Images of at least 2 randomly
619 selected fields of view were acquired using Z-stacks separated by 1 μ m. For each
620 condition, at least two independent experiments were performed. Statistical analysis
621 was done using the Student's t-test.

622 GUVs containing IFITM3 protein were prepared through dehydration of IFITM3-
623 containing LUVs, as previously described (Girard et al., 2004). Briefly, IFITM3-
624 containing LUVs were prepared, as above, added dropwise onto indium-tin oxide

625 coated slides, and dehydrated under vacuum overnight. The lipids were rehydrated and
626 electroformed, as described above at room temperature for 6 h.

627 **Plasma membrane spheres**

628 Plasma membrane spheres were prepared as previously described (Lingwood et al.,
629 2008). Briefly, A549 cells transduced with IFITM3-iSNAP/pQCXIP expression vector
630 were seeded on 8-well chambered coverslip. 24 h later cells were washed and incubated
631 for 18 hr in PMS buffer (1.5 mM CaCl₂, 1.5 mM MgCl₂, 5 mM HEPES pH 7.4, 1 mg/ml
632 glucose in 1x PBS) at 37 °C. The lipid ordered phase was visualized through GM1
633 crosslinking by incubating the PMS in 10 µg/ml of Alexa-488 labeled cholera-toxin
634 subunit B (Invitrogen) for 2 h at 37°C and IFITM3-iSNAP was stained with 3 µM
635 SNAP-cell 647-SIR (New England Biolabs) at the same time. PMS were then washed
636 and imaged at room temperature on a Zeiss LSM880 laser scanning confocal
637 microscopes, using a 63x/1.4NA oil-immersion objective.

638 **Lipid mixing between influenza virus and GUVs**

639 Virus labeling was performed essentially as described previously (Suddala et al., 2019).
640 Briefly, a 100 µl aliquot of the 2 mg/ml Influenza A/PR/8/34 virus stock (Charles River,
641 CT, USA) was thawed at room temperature and diluted using 50 µl isotonic 145 mM
642 NaCl/50 mM HEPES (pH 7.4) buffer. To label the virus membrane, 1.5 µl of DiD dye
643 (Invitrogen, 10 mM stock solution in DMSO) was quickly injected into a mixture
644 during mild vortexing to final concentration of 100 µM. The tube was closed, wrapped
645 with aluminum foil and agitated at the lowest speed setting of a vortex for 1 hour at
646 room temperature. The labeled viruses were purified from excess dyes on a Nap-5 gel
647 filtration column (GE Healthcare) that was equilibrated with 50 mM HEPES, pH 7.4,
648 145 mM NaCl at room temperature. The fractions containing labeled viruses were
649 passed through a 0.45 µm filter to remove any large lipid and/or virus aggregates. To
650 test the labeling efficiency, 10 µl of the purified viruses were diluted to 1000 µl in PBS,
651 lysed with 0.5% TX-100 (final concentration) and the extent of DiD dequenching was
652 measured in a plate reader. A more than 20-fold increase in the DiD signal upon lysis
653 has been found to give good results in lipid mixing experiments. The labeled virus was
654 aliquoted into tubes, flash-frozen, and stored at -80 °C until use. The virus lipid mixing
655 assay was performed by mixing 20 µl of the labeled virus with 30 µl GUVs, followed

656 by addition of 150 μ l of 100 mM citrate buffer (pH 4.8) supplemented with 100 mM
657 MES to achieve the final pH of 5.0. The resulting mixture was transferred into a BSA-
658 pretreated 8-well coverslip and imaged on a Zeiss LSM880 laser scanning confocal
659 microscope, using a 63x/1.4NA oil-immersion objective.

660

661 **Lipid order measurement**

662 To assess the lipid order, 2 mM of LUVs were mixed with 25 μ M of Laurdan dye
663 (Invitrogen) and 40 μ M of indicated IFITM3-derived peptide in a total volume of 50 μ l.
664 Fluorescence was measured on a SpectraMax i3x microplate reader using a 355 nm
665 excitation filter and recording fluorescence emissions at two wavelengths centered at
666 440 and 490 nm. Laurdan general polarization (GP) was calculated using the equation:
667 $GP = (I_{440} - I_{490}) / (I_{440} + I_{490})$, where I_{440} and I_{490} are fluorescence intensities at 440 nm and
668 490 nm, respectively.

669 **Membrane bending rigidity measurement**

670 GUVs were grown on a polyvinyl alcohol (PVA) film as described previously
671 (Weinberger et al., 2013). Briefly, 50 μ l of 5% w/v (145000 g/mol) PVA (Merck)
672 solution in water was spread on a cleaned (rinsed in ethanol and double distilled water)
673 glass slide to form a thin film. The PVA film was dried kept in the oven at 50°C for 30
674 minutes. Five μ l of 2 mM lipid solution (80 mol % POPC, 20 mol % cholesterol) in
675 chloroform was spread on the PVA film and the solvent was evaporated in vacuum for
676 1 hour. An observation chamber with a volume of about 700 μ l was assembled using a
677 Teflon spacer sandwiched between two glasses with the lipid film facing inward, and
678 the lipid films were hydrated in solution of 100 mM sucrose (Sigma), 1 mM HEPES
679 (Sigma) at pH 7.4. After swelling for 30 minutes, GUVs were harvested and used right
680 away. An aliquot of 0.1 μ l DMSO solution with or without the peptide was carefully
681 pipetted into 100 μ l GUV suspension and slowly agitated to ensure mixing.
682 Subsequently, 30 μ l of the final solution was placed on a BSA coated glass coverslip.
683 A few percent of the solution was left to evaporate for three to five minutes to ambient
684 air and then closed in an observation chamber. Bending rigidity analysis was performed
685 either on vesicles with added DMSO only (control) or DMSO with IFITM3 at final
686 concentration of the peptide of 3 nM. Membrane bending rigidity was measured by
687 fluctuation analysis of the thermally induced motion of the membrane, as described

688 previously (Gracia et al., 2010). Experiments were performed on an Axio Observer D1
689 microscope (Zeiss, Germany) using a 40× objective in phase contrast mode. Imaging
690 was performed using a low noise liquid-cooled digital camera pco.edge 5.5 a total of
691 1000-2000 snapshots per vesicle were acquired with exposure time of 200 μs at 10
692 frames per second.

693

694 **Virus infection assay**

695 Luciferase-expressing pseudoviruses were produced by transfecting HEK293T/17 cells
696 using JetPRIME transfection reagent (Polyplus-transfection, SA, NY), as described
697 previously (Francis, Marin, Shi, Aiken, & Melikyan, 2016). Briefly, HEK293T/17 cells
698 grown in a 100-mm dish were transfected with 2.5 μg of pCAGGS plasmid expressing
699 H1N1 HA and NA proteins, 4 μg NL4-3R⁺E⁻Luc, and 1 μg pcRev. The transfection
700 medium was replaced with fresh DMEM/10% FBS after 12 h, and cells were cultured
701 for additional 36 h, after which time, the virus-containing culture medium was collected,
702 passed through a 0.45-μm filter, and concentrated 10x using Lenti-X Concentrator
703 (Clontech, Mountain View, CA). Following an overnight concentration with Lenti-X,
704 virus was precipitated by centrifuging at 1439×g for 45 min at 4°C, resuspended in
705 DMEM without phenol red or FBS, and stored at -80 °C. Infection assays were
706 performed using HEK 293T/17 cells transfected with indicated IFITM3 constructs in
707 pcDNA3.1(+) vector using JetPRIME transfection reagent. At 24 h post-transfection,
708 pseudoviruses (0.1 ng of p24) were spinoculated onto cells at 1,500×g, 4°C for 30 min,
709 and cells were cultured for 24 h. Luciferase activity was determined by adding Bright-
710 Glo Luciferase substrate (Promega, WI, USA) and reading with a TopCount NXT
711 Luminescence counter (PerkinElmer, Waltham, MA, USA).

712 For infection of mCherry-expressing IAV PR8 virus, HEK 293T/17 cells were seeded
713 on 8-well chambered coverslip 24 h before transfection with indicated IFITM3
714 constructs in pQCXIP. At 12 h post-transfection, mCherry-expressing IAV PR8 virus
715 (2.5×10^4 PFU/ml) was spinoculated onto cells at 1,500×g, 4°C for 30 min, and cells
716 were cultured for 12 h and imaged on a Zeiss LSM880 laser scanning confocal
717 microscope, using a 20x objective.

718

719 **Insulin secretion assay**

720 An insulin secretion assay was performed, as described previously (Burns et al., 2015)
721 with some modifications. Briefly, A lentivirus vector expressing luciferase fusion
722 protein was produced using a second-generation viral packaging system. 4 µg of
723 pLX304 vector containing the fusion construct Proinsulin-NanoLuc, 2 µg of psPAX2
724 packaging plasmid, 2 µg of pMD2.G envelope plasmid were used to transfect a 10 cm
725 dish of HEK 293T/17cells using JetPRIME transfection reagent. Virus was harvested
726 at 48 hours post-transfection and passed through 0.45 µm cellulose acetate filters prior
727 to use. Viruses were spun onto INS-1E cells at 800 xg for 1 hour at 30 °C. After 24
728 hours at 37 °C in 5% CO₂ in the presence of virus, the medium was placed in fresh
729 growth media with 5 µg/mL blasticidin (Invitrogen) for 3 days to select for infected
730 cells. For insulin secretion assays, INS-1E cells were plated in 96-well plates and
731 cultured overnight at 37 °C in 5% CO₂. Cells were washed once with PBS and incubated
732 for 1 hour at 37 °C in sterile, 0.45 µm-filtered Krebs Ringer Buffer (KRB) containing
733 138 mM NaCl, 5.4 mM KCl, 2.6 mM MgCl₂, 2.6 mM CaCl₂, 5 mM NaHCO₃, 10 mM
734 HEPES and 5 g/L BSA (Sigma), supplemented with 2.8 mM glucose. The cells were
735 then incubated with 2 µM of indicated IFITM3 peptides in KRB for 5 min and then
736 stimulated for 20 mins in 100 µl of fresh KRB with 20 mM glucose. For the time course
737 study, after incubating the cells for one hour in 2.8 mM glucose KRB, the buffer was
738 changed every 5 minutes to fresh, prewarmed to 37 °C KRB containing either 2.8 mM
739 glucose (for the first time point) or 20 mM glucose (for all subsequent time points).
740 The luciferase signal in samples was determined by adding the coelenterazine substrate
741 (NanoLight, Pinetop, AZ) to the supernatant to a final concentration of 10 µM and
742 reading on a TopCount NXT Luminescence counter.

743

744 **Acknowledgments**

745 We gratefully acknowledge lab members, Drs. Yen-Cheng Chen and Ashwanth Francis
746 for assistance with GUV imaging, Dr. You Zhang for functional test of IFITM3-iSNAP
747 and advice on the labeling procedure, Ms. Teddy Khan for assistance with molecular
748 cloning, and Mrs. Hui Wu for assistance with cell culture. We thank Henry Cho
749 (Addexbio Technologies) for technical support with INS-1E cells culture and handling
750 and Dr. Zachary Freyberg (University of Pittsburgh) for advice on handling insulin-
751 secreting cells. We also thank Weirong Yuan (University of Maryland) for technical

752 help with peptide synthesis. This work was funded by the NIH R01 grant AI135806 to
753 G.B.M. J.S. and R.D. thank the MaxSynBio consortium, which is jointly funded by the
754 Federal Ministry of Education and Research (BMBF) of Germany and the Max Planck
755 Society (MPG).

756

757 **Author Contributions**

758 XG and GBM conceived this study; XG, JS and MM performed the experiments; WL
759 and XL provided reagents; RD advised on bending modulus measurements; XG and
760 GBM wrote the first draft of the manuscript; all authors read and edited the manuscript.

761

762 **Declaration of Interests:** The authors declare no competing interests.

763

764 **References**

765

766 Amatore, C., Arbault, S., Bouret, Y., Guille, M., Lemaitre, F., & Verchier, Y. (2006).

767 Regulation of exocytosis in chromaffin cells by trans-insertion of
768 lysophosphatidylcholine and arachidonic acid into the outer leaflet of the cell
769 membrane. *Chembiochem*, 7(12), 1998-2003. doi:10.1002/cbic.200600194

770 Amini-Bavil-Olyaei, S., Choi, Y. J., Lee, J. H., Shi, M., Huang, I. C., Farzan, M., &

771 Jung, J. U. (2013). The antiviral effector IFITM3 disrupts intracellular

772 cholesterol homeostasis to block viral entry. *Cell Host Microbe*, 13(4), 452-

773 464. doi:10.1016/j.chom.2013.03.006

774 Angelova, M. I., & Dimitrov, D. S. (1986). Liposome Electroformation. *Faraday*

775 *Discussions*, 81, 303-+. doi:DOI 10.1039/dc9868100303

776 Appourchaux, R., Delpuech, M., Zhong, L., Burlaud-Gaillard, J., Tartour, K., Savidis,

777 G., . . . Cimarelli, A. (2019). Functional Mapping of Regions Involved in the

778 Negative Imprinting of Virion Particle Infectivity and in Target Cell

779 Protection by Interferon-Induced Transmembrane Protein 3 against HIV-1. *J*

780 *Virology*, 93(2). doi:10.1128/JVI.01716-18

781 Bailey, C. C., Huang, I. C., Kam, C., & Farzan, M. (2012). Ifitm3 limits the severity

782 of acute influenza in mice. *PLoS Pathog*, 8(9), e1002909.

783 doi:10.1371/journal.ppat.1002909

784 Bailey, C. C., Kondur, H. R., Huang, I. C., & Farzan, M. (2013). Interferon-induced

785 transmembrane protein 3 is a type II transmembrane protein. *J Biol Chem*,

786 288(45), 32184-32193. doi:10.1074/jbc.M113.514356

787 Bassereau, P., Jin, R., Baumgart, T., Deserno, M., Dimova, R., Frolov, V. A., . . .

788 Weikl, T. R. (2018). The 2018 biomembrane curvature and remodeling

789 roadmap. *J Phys D Appl Phys*, 51(34). doi:10.1088/1361-6463/aac998

790 Brass, A. L., Huang, I. C., Benita, Y., John, S. P., Krishnan, M. N., Feeley, E. M., . . .

791 Elledge, S. J. (2009). The IFITM proteins mediate cellular resistance to

792 influenza A H1N1 virus, West Nile virus, and dengue virus. *Cell*, 139(7),

793 1243-1254. doi:10.1016/j.cell.2009.12.017

794 Burns, S. M., Vetere, A., Walpita, D., Dancik, V., Khodier, C., Perez, J., . . .

795 Altshuler, D. (2015). High-throughput luminescent reporter of insulin

- 796 secretion for discovering regulators of pancreatic Beta-cell function. *Cell*
797 *Metab*, 21(1), 126-137. doi:10.1016/j.cmet.2014.12.010
- 798 Chazal, N., & Gerlier, D. (2003). Virus entry, assembly, budding, and membrane
799 rafts. *Microbiology and Molecular Biology Reviews*, 67(2), 226-+.
800 doi:10.1128/Mmbr.67.2.226-237.2003
- 801 Chernomordik, L. V., Frolov, V. A., Leikina, E., Bronk, P., & Zimmerberg, J. (1998).
802 The pathway of membrane fusion catalyzed by influenza hemagglutinin:
803 restriction of lipids, hemifusion, and lipidic fusion pore formation. *J Cell Biol*,
804 140(6), 1369-1382. doi:10.1083/jcb.140.6.1369
- 805 Chernomordik, L. V., & Kozlov, M. M. (2003). Protein-lipid interplay in fusion and
806 fission of biological membranes. *Annu Rev Biochem*, 72, 175-207.
- 807 Chernomordik, L. V., Leikina, E., Frolov, V., Bronk, P., & Zimmerberg, J. (1997). An
808 early stage of membrane fusion mediated by the low pH conformation of
809 influenza hemagglutinin depends upon membrane lipids. *J Cell Biol*, 136(1),
810 81-93. doi:10.1083/jcb.136.1.81
- 811 Chernomordik, L. V., Melikyan, G. B., & Chizmadzhev, Y. A. (1987). Biomembrane
812 fusion: a new concept derived from model studies using two interacting planar
813 lipid bilayers. *Biochim Biophys Acta*, 906(3), 309-352.
- 814 Chesarino, N. M., Compton, A. A., McMichael, T. M., Kenney, A. D., Zhang, L.,
815 Soewarna, V., . . . Yount, J. S. (2017). IFITM3 requires an amphipathic helix
816 for antiviral activity. *EMBO Rep*, 18(10), 1740-1751.
817 doi:10.15252/embr.201744100
- 818 Desai, T. M., Marin, M., Chin, C. R., Savidis, G., Brass, A. L., & Melikyan, G. B.
819 (2014). IFITM3 restricts influenza A virus entry by blocking the formation of
820 fusion pores following virus-endosome hemifusion. *PLoS Pathog*, 10(4),
821 e1004048. doi:10.1371/journal.ppat.1004048
- 822 Diamond, M. S., & Farzan, M. (2013). The broad-spectrum antiviral functions of IFIT
823 and IFITM proteins. *Nat Rev Immunol*, 13(1), 46-57. doi:10.1038/nri3344
- 824 Drin, G., & Antonny, B. (2010). Amphipathic helices and membrane curvature. *Febs*
825 *Letters*, 584(9), 1840-1847. doi:10.1016/j.febslet.2009.10.022
- 826 Everitt, A. R., Clare, S., McDonald, J. U., Kane, L., Harcourt, K., Ahras, M., . . .
827 Kellam, P. (2013). Defining the range of pathogens susceptible to Ifitm3

- 828 restriction using a knockout mouse model. *PLoS One*, 8(11), e80723.
829 doi:10.1371/journal.pone.0080723
- 830 Everitt, A. R., Clare, S., Pertel, T., John, S. P., Wash, R. S., Smith, S. E., . . . Kellam,
831 P. (2012). IFITM3 restricts the morbidity and mortality associated with
832 influenza. *Nature*, 484(7395), 519-523. doi:10.1038/nature10921
- 833 Feeley, E. M., Sims, J. S., John, S. P., Chin, C. R., Pertel, T., Chen, L. M., . . . Brass,
834 A. L. (2011). IFITM3 inhibits influenza A virus infection by preventing
835 cytosolic entry. *PLoS Pathog*, 7(10), e1002337.
836 doi:10.1371/journal.ppat.1002337
- 837 Francis, A. C., Marin, M., Shi, J., Aiken, C., & Melikyan, G. B. (2016). Time-
838 Resolved Imaging of Single HIV-1 Uncoating In Vitro and in Living Cells.
839 *PLoS Pathog*, 12(6), e1005709. doi:10.1371/journal.ppat.1005709
- 840 Fu, B., Wang, L., Li, S., & Dorf, M. E. (2017). ZMPSTE24 defends against influenza
841 and other pathogenic viruses. *J Exp Med*, 214(4), 919-929.
842 doi:10.1084/jem.20161270
- 843 Fuller, N., & Rand, R. P. (2001). The influence of lysolipids on the spontaneous
844 curvature and bending elasticity of phospholipid membranes. *Biophysical*
845 *Journal*, 81(1), 243-254. doi:Doi 10.1016/S0006-3495(01)75695-0
- 846 Girard, P., Pecreaux, J., Lenoir, G., Falson, P., Rigaud, J. L., & Bassereau, P. (2004).
847 A new method for the reconstitution of membrane proteins into giant
848 unilamellar vesicles. (vol 87, pg 419, yr 2004). *Biophysical Journal*, 87(3),
849 2098-2098. doi:10.1529/biophysj.104.900104
- 850 Gracia, R. S., Bezlyepkina, N., Knorr, R. L., Lipowsky, R., & Dimova, R. (2010).
851 Effect of cholesterol on the rigidity of saturated and unsaturated membranes:
852 fluctuation and electrodeformation analysis of giant vesicles. *Soft Matter*, 6(7),
853 1472-1482. doi:10.1039/b920629a
- 854 Harrison, S. C. (2008). Viral membrane fusion. *Nat Struct Mol Biol*, 15(7), 690-698.
855 doi:10.1038/nsmb.1456
- 856 Helfrich, W. (1973). Elastic Properties of Lipid Bilayers - Theory and Possible
857 Experiments. *Zeitschrift Fur Naturforschung C-a Journal of Biosciences*, C
858 28(11-1), 693-703. doi:DOI 10.1515/znc-1973-11-1209

- 859 Huang, I. C., Bailey, C. C., Weyer, J. L., Radoshitzky, S. R., Becker, M. M., Chiang,
860 J. J., . . . Farzan, M. (2011). Distinct patterns of IFITM-mediated restriction of
861 filoviruses, SARS coronavirus, and influenza A virus. *PLoS Pathog*, 7(1),
862 e1001258. doi:10.1371/journal.ppat.1001258
- 863 Jia, R., Xu, F. W., Qian, J., Yao, Y. F., Miao, C. H., Zheng, Y. M., . . . Liang, C.
864 (2014). Identification of an endocytic signal essential for the antiviral action of
865 IFITM3. *Cellular Microbiology*, 16(7), 1080-1093. doi:10.1111/cmi.12262
- 866 John, S. P., Chin, C. R., Perreira, J. M., Feeley, E. M., Aker, A. M., Savidis, G., . . .
867 Brass, A. L. (2013). The CD225 domain of IFITM3 is required for both
868 IFITM protein association and inhibition of influenza A virus and dengue
869 virus replication. *J Virol*, 87(14), 7837-7852. doi:10.1128/JVI.00481-13
- 870 Julkowska, M. M., Rankenberg, J. M., & Testerink, C. (2013). Liposome-binding
871 assays to assess specificity and affinity of phospholipid-protein interactions.
872 *Methods Mol Biol*, 1009, 261-271. doi:10.1007/978-1-62703-401-2_24
- 873 Kaiser, H. J., Lingwood, D., Levental, I., Sampaio, J. L., Kalvodova, L., Rajendran,
874 L., & Simons, K. (2009). Order of lipid phases in model and plasma
875 membranes. *Proceedings of the National Academy of Sciences of the United*
876 *States of America*, 106(39), 16645-16650. doi:10.1073/pnas.0908987106
- 877 Karimi, M., Steinkuhler, J., Roy, D., Dasgupta, R., Lipowsky, R., & Dimova, R.
878 (2018). Asymmetric Ionic Conditions Generate Large Membrane Curvatures.
879 *Nano Lett*, 18(12), 7816-7821. doi:10.1021/acs.nanolett.8b03584
- 880 Kozlov, M. M. (2007). Determination of lipid spontaneous curvature from X-ray
881 examinations of inverted hexagonal phases. *Methods Mol Biol*, 400, 355-366.
882 doi:10.1007/978-1-59745-519-0_24
- 883 Kozlov, M. M., Leikin, S. L., Chernomordik, L. V., Markin, V. S., & Chizmadzhev,
884 Y. A. (1989). Stalk mechanism of vesicle fusion. Intermixing of aqueous
885 contents. *Eur Biophys J*, 17(3), 121-129. doi:10.1007/BF00254765
- 886 Levental, I., Lingwood, D., Grzybek, M., Coskun, U., & Simons, K. (2010).
887 Palmitoylation regulates raft affinity for the majority of integral raft proteins.
888 *Proceedings of the National Academy of Sciences of the United States of*
889 *America*, 107(51), 22050-22054. doi:10.1073/pnas.1016184107

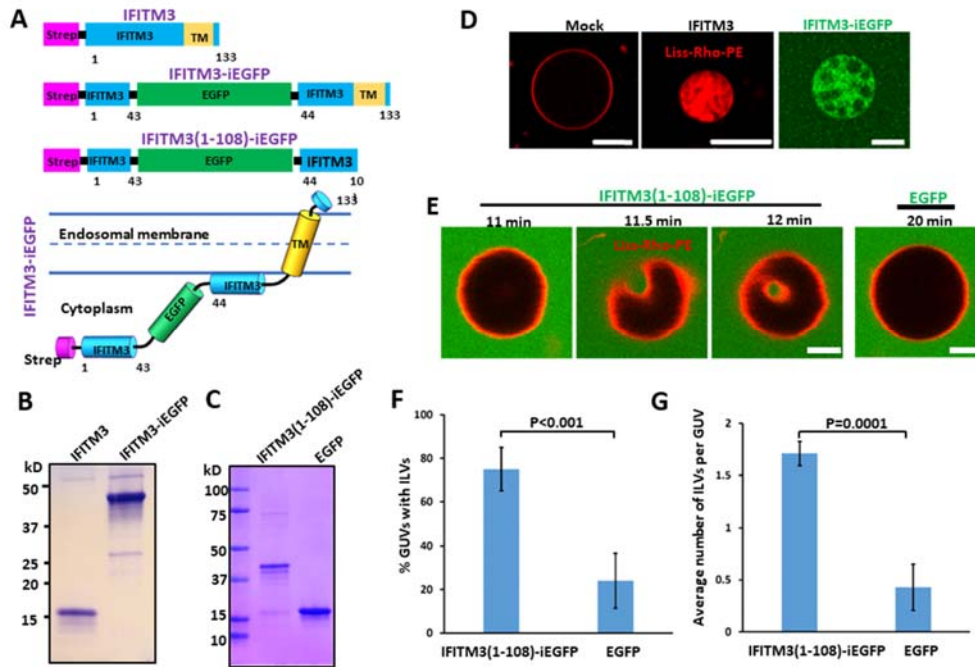
- 890 Li, K., Markosyan, R. M., Zheng, Y. M., Golfetto, O., Bungart, B., Li, M., . . . Liu, S.
891 L. (2013). IFITM proteins restrict viral membrane hemifusion. *PLoS Pathog*,
892 9(1), e1003124. doi:10.1371/journal.ppat.1003124
- 893 Lin, T. Y., Chin, C. R., Everitt, A. R., Clare, S., Ferreira, J. M., Savidis, G., . . . Brass,
894 A. L. (2013). Amphotericin B increases influenza A virus infection by
895 preventing IFITM3-mediated restriction. *Cell Rep*, 5(4), 895-908.
896 doi:10.1016/j.celrep.2013.10.033
- 897 Ling, S., Zhang, C., Wang, W., Cai, X., Yu, L., Wu, F., . . . Tian, C. (2016).
898 Combined approaches of EPR and NMR illustrate only one transmembrane
899 helix in the human IFITM3. *Sci Rep*, 6, 24029. doi:10.1038/srep24029
- 900 Lingwood, D., Ries, J., Schwille, P., & Simons, K. (2008). Plasma membranes are
901 poised for activation of raft phase coalescence at physiological temperature.
902 *Proceedings of the National Academy of Sciences of the United States of*
903 *America*, 105(29), 10005-10010. doi:10.1073/pnas.0804374105
- 904 Martyna, A., Bahsoun, B., Badham, M. D., Srinivasan, S., Howard, M. J., &
905 Rossman, J. S. (2017). Membrane remodeling by the M2 amphipathic helix
906 drives influenza virus membrane scission. *Scientific Reports*, 7. doi:ARTN
907 44695
908 10.1038/srep44695
- 909 McMahon, H. T., & Gallop, J. L. (2005). Membrane curvature and mechanisms of
910 dynamic cell membrane remodelling. *Nature*, 438(7068), 590-596.
911 doi:10.1038/nature04396
- 912 Merglen, A., Theander, S., Rubi, B., Chaffard, G., Wollheim, C. B., & Maechler, P.
913 (2004). Glucose sensitivity and metabolism-secretion coupling studied during
914 two-year continuous culture in INS-1E insulinoma cells. *Endocrinology*,
915 145(2), 667-678. doi:10.1210/en.2003-1099
- 916 Mudhasani, R., Tran, J. P., Retterer, C., Radoshitzky, S. R., Kota, K. P., Altamura, L.
917 A., . . . Bavari, S. (2013). IFITM-2 and IFITM-3 but not IFITM-1 restrict Rift
918 Valley fever virus. *J Virol*, 87(15), 8451-8464. doi:10.1128/JVI.03382-12
- 919 Parasassi, T., De Stasio, G., Dubaldo, A., & Gratton, E. (1990). Phase Fluctuation in
920 Phospholipid-Membranes Revealed by Laurdan Fluorescence. *Biophysical*
921 *Journal*, 57(6), 1179-1186. doi:Doi 10.1016/S0006-3495(90)82637-0

- 922 Rajendran, L., & Simons, K. (2005a). Lipid rafts and membrane dynamics. *Journal of*
923 *Cell Science*, *118*(6), 1099-1102. doi:10.1242/jcs.01681
- 924 Rajendran, L., & Simons, K. (2005b). Lipid rafts and membrane dynamics. *Journal of*
925 *Cell Science*, *118*(Pt 6), 1099-1102. doi:10.1242/jcs.01681
- 926 Rigaud, J. L., & Levy, D. (2003). Reconstitution of membrane proteins into
927 liposomes. *Liposomes, Pt B*, *372*, 65-86. Retrieved from <Go to
928 ISI>://WOS:000186734500004
- 929 Rossman, J. S., Jing, X. H., Leser, G. P., & Lamb, R. A. (2010). Influenza Virus M2
930 Protein Mediates ESCRT-Independent Membrane Scission. *Cell*, *142*(6), 902-
931 913. doi:10.1016/j.cell.2010.08.029
- 932 Stachowiak, J. C., Hayden, C. C., & Sasaki, D. Y. (2010). Steric confinement of
933 proteins on lipid membranes can drive curvature and tubulation. *Proceedings*
934 *of the National Academy of Sciences of the United States of America*, *107*(17),
935 7781-7786. doi:10.1073/pnas.0913306107
- 936 Steinkuhler, J., Knorr, R. L., Zhao, Z., Bhatia, T., Bartelt, S. M., Wegner, S., . . .
937 Lipowsky, R. (2020). Controlled division of cell-sized vesicles by low
938 densities of membrane-bound proteins. *Nat Commun*, *11*(1), 905.
939 doi:10.1038/s41467-020-14696-0
- 940 Steinkuhler, J., Sezgin, E., Urbancic, I., Eggeling, C., & Dimova, R. (2019).
941 Mechanical properties of plasma membrane vesicles correlate with lipid order,
942 viscosity and cell density. *Communications Biology*, *2*. doi:UNSP 337
943 10.1038/s42003-019-0583-3
- 944 Stiasny, K., & Heinz, F. X. (2004). Effect of membrane curvature-modifying lipids on
945 membrane fusion by tick-borne encephalitis virus. *J Virol*, *78*(16), 8536-8542.
946 doi:10.1128/JVI.78.16.8536-8542.2004
- 947 Suddala, K. C., Lee, C. C., Meraner, P., Marin, M., Markosyan, R. M., Desai, T.
948 M., . . . Melikyan, G. B. (2019). Interferon-induced transmembrane protein 3
949 blocks fusion of sensitive but not resistant viruses by partitioning into virus-
950 carrying endosomes. *PLoS Pathog*, *15*(1), e1007532.
951 doi:10.1371/journal.ppat.1007532
- 952 Tartour, K., Nguyen, X. N., Appourchaux, R., Assil, S., Barateau, V., Bloyet, L.
953 M., . . . Cimorelli, A. (2017). Interference with the production of infectious

- 954 viral particles and bimodal inhibition of replication are broadly conserved
955 antiviral properties of IFITMs. *PLoS Pathog*, 13(9), e1006610.
956 doi:10.1371/journal.ppat.1006610
- 957 Vanblitterswijk, W. J., Vanhoeven, R. P., & Vandermeer, B. W. (1981). Lipid
958 Structural Order Parameters (Reciprocal of Fluidity) in Biomembranes
959 Derived from Steady-State Fluorescence Polarization Measurements.
960 *Biochimica Et Biophysica Acta*, 644(2), 323-332. doi:Doi 10.1016/0005-
961 2736(81)90390-4
- 962 Weinberger, A., Tsai, F. C., Koenderink, G. H., Schmidt, T. F., Itri, R., Meier, W., . . .
963 Marques, C. (2013). Gel-assisted formation of giant unilamellar vesicles.
964 *Biophysical Journal*, 105(1), 154-164. doi:10.1016/j.bpj.2013.05.024
- 965 Wesolowska, O., Michalak, K., Maniewska, J., & Hendrich, A. B. (2009). Giant
966 unilamellar vesicles - a perfect tool to visualize phase separation and lipid
967 rafts in model systems. *Acta Biochimica Polonica*, 56(1), 33-39. Retrieved
968 from <Go to ISI>://WOS:000264798400004
- 969 Wrensch, F., Winkler, M., & Pohlmann, S. (2014). IFITM Proteins Inhibit Entry
970 Driven by the MERS-Coronavirus Spike Protein: Evidence for Cholesterol-
971 Independent Mechanisms. *Viruses*, 6(9), 3683-3698. doi:10.3390/v6093683
- 972 Wu, X., Spence, J. S., Das, T., Yuan, X., Chen, C., Zhang, Y., . . . Peng, T. (2020).
973 Site-Specific Photo-Crosslinking Proteomics Reveal Regulation of IFITM3
974 Trafficking and Turnover by VCP/p97 ATPase. *Cell Chem Biol*.
975 doi:10.1016/j.chembiol.2020.03.004
- 976 Yang, S. T., Kreuzberger, A. J. B., Kiessling, V., Ganser-Pornillos, B. K., White, J.
977 M., & Tamm, L. K. (2017). HIV virions sense plasma membrane
978 heterogeneity for cell entry. *Science Advances*, 3(6). doi:ARTN e1700338
979 10.1126/sciadv.1700338
- 980 Yount, J. S., Moltedo, B., Yang, Y. Y., Charron, G., Moran, T. M., Lopez, C. B., &
981 Hang, H. C. (2010). Palmitoylome profiling reveals S-palmitoylation-
982 dependent antiviral activity of IFITM3. *Nature Chemical Biology*, 6(8), 610-
983 614. doi:10.1038/Nchembio.405
- 984 Zhang, Y. H., Zhao, Y., Li, N., Peng, Y. C., Giannoulatou, E., Jin, R. H., . . . Dong, T.
985 (2013). Interferon-induced transmembrane protein-3 genetic variant rs12252-

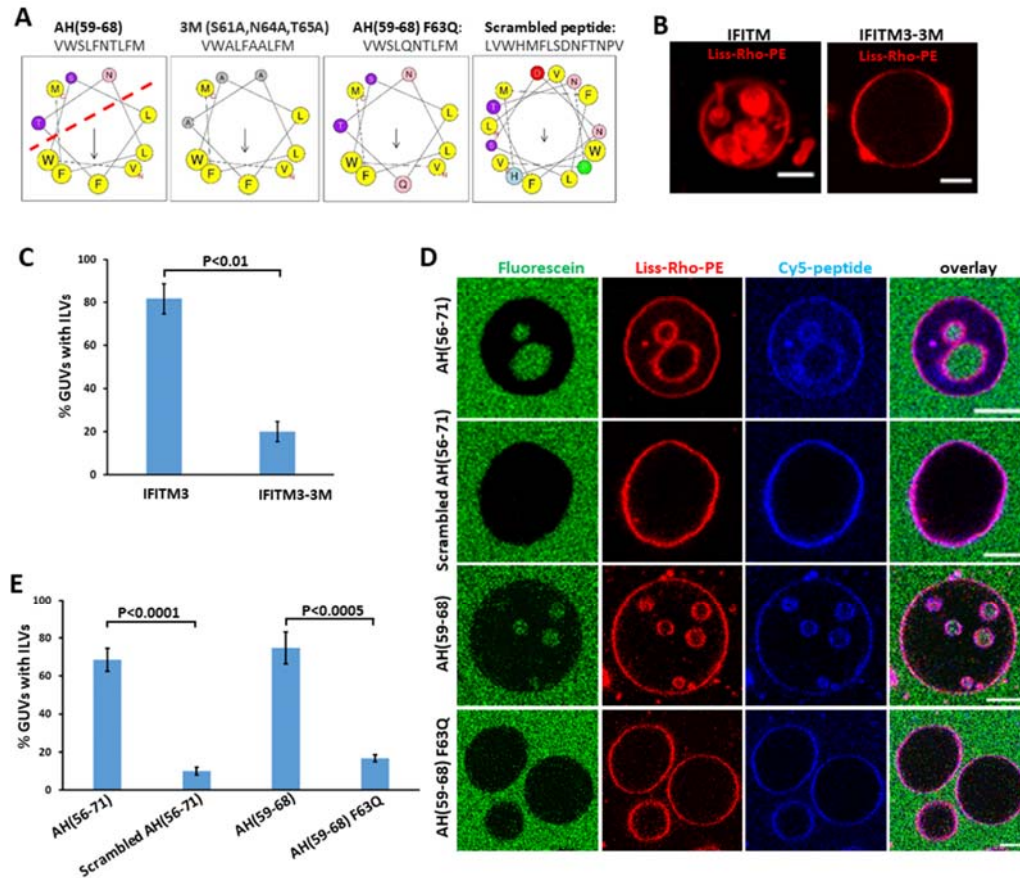
986 C is associated with severe influenza in Chinese individuals. *Nat Commun*, 4,
987 1418. doi:10.1038/ncomms2433
988 Zhang, Z., Liu, J., Li, M., Yang, H., & Zhang, C. (2012). Evolutionary dynamics of
989 the interferon-induced transmembrane gene family in vertebrates. *PLoS One*,
990 7(11), e49265. doi:10.1371/journal.pone.0049265
991
992

993 **Figures and Figure Legends**



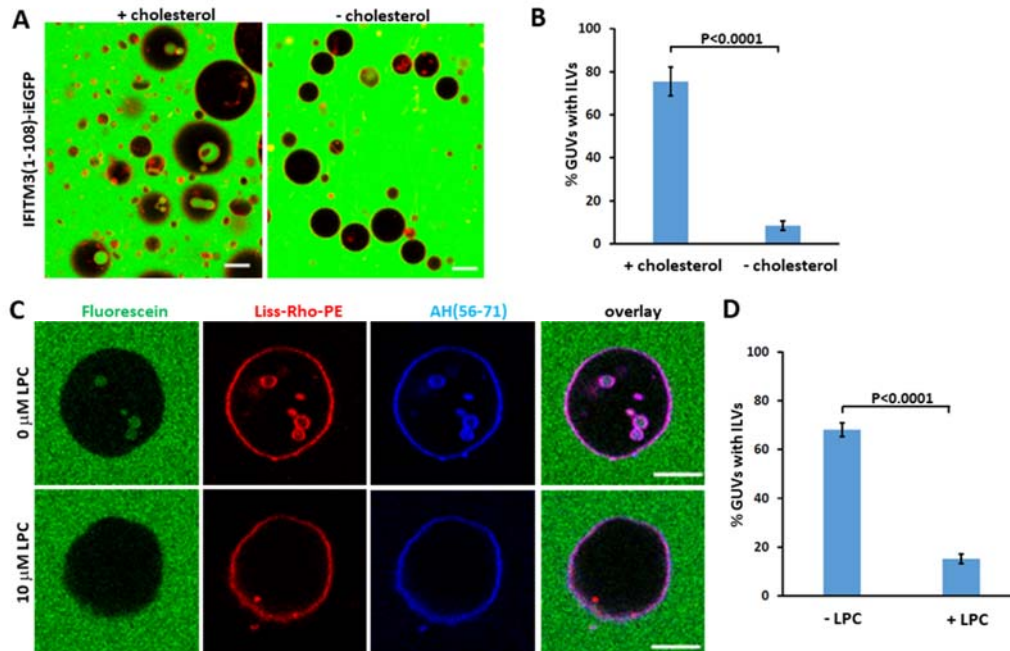
994
995 **Figure 1. IFITM3 induces negative membrane curvature *in vitro*.** (A) Illustration
996 of domains of recombinant IFITM3 with an N-terminal Strep tag (IFITM3), Strep-
997 tagged IFITM3 with an internal GFP tag (IFITM3-iEGFP), and C-terminally truncated
998 IFITM3 lacking the transmembrane domain (TM) with Strep tag and internal GFP tags
999 (IFITM3(1-108)-iEGFP). Lower cartoon illustrates the membrane topology of IFITM-
1000 iEGFP. The numbers indicate the amino acid numbers. (B, C) SDS-PAGE analysis and
1001 Coomassie blue staining of purified IFITM3 recombinant proteins shown in A. (D)
1002 IFITM3- and IFITM3-iEGFP-reconstituted LUVs (99.0 mol % POPC, 0.5 mol %
1003 cholesterol, 0.5 mol % Liss-Rho-PE) were dehydrated, electroformed into GUVs, and
1004 immediately imaged. Fluorescent Liss-Rho-PE lipid is shown in red. Scale bars 20 μ m.
1005 (E) Time-lapse images of a GUV (99.0 mol % POPC, 0.5 mol % cholesterol, 0.5 mol %
1006 Liss-Rho-PE) incubated with 20 μ M IFITM3(1-108)-iEGFP showing an inward
1007 budding of GUV membrane. A control GUV (right) was incubated with 20 μ M EGFP
1008 and imaged under the same condition. Scale bars 5 μ m. (F) Quantification of IFITM3-
1009 induced inward budding plotted as the percentage of GUVs with at least one IFITM3(1-
1010 108)-iEGFP or EGFP-filled intraluminal vesicle (ILV). Data represent mean \pm SD from
1011 two independent experiments. At least 50 GUVs were analyzed per sample in each
1012 experiment. (G) Same as in (F), but the plotted values represent the average number of
1013 ILVs per GUV. See also Figure S1.

1014



1015

1016 **Figure 2. IFITM3 amphipathic helix is responsible for induction of negative**
 1017 **membrane curvature.** (A) Sequences and helical wheel projection plots created for
 1018 IFITM3 AH and mutants using HELIQUEST software. Hydrophobic residues are
 1019 displayed as gray or yellow, while hydrophilic residues are displayed as pink or purple.
 1020 Arrows represent the magnitude and orientation of the mean hydrophobic moment
 1021 value calculated by HELIQUEST software. (B) IFITM3- and IFITM3-3M-
 1022 reconstituted LUVs were dehydrated, electroformed into GUVs and immediately
 1023 imaged. Scale bars 10 μ m. (C) The percentage of GUVs, prepared and treated as in (B),
 1024 containing at least one ILV. Data represent mean \pm SD from two independent
 1025 experiments, with at least 30 GUVs analyzed per sample in each experiment. (D) GUVs
 1026 were treated with 10 μ M AH(56-71), 10 μ M Scrambled AH(56-71), 10 μ M AH(59-68)
 1027 or 30 μ M AH(59-68) F63Q for 30 min and imaged. 0.3 μ M fluorescein was added to
 1028 the external buffer to mark *bona fide* inward budding of GUVs. Scale bars 10 μ m. (E)
 1029 Percentage of GUVs, prepared and treated as in (D), with at least one ILV containing
 1030 fluorescein. Data represent mean \pm SD of the results of three independent experiments,
 1031 with at least 90 GUVs counted per sample in each experiment. See also Figure S2.



1032

1033

Figure 3. Negative membrane curvature induced by IFITM3 is facilitated by

1034

cholesterol and counteracted by lyso-lipids. (A) GUVs with cholesterol (99.0 mol %

1035

POPC, 0.5 mol % cholesterol, 0.5 mol % Liss-Rho-PE) or GUVs without cholesterol

1036

(99.5 mol % POPC, 0.5 mol % Liss-Rho-PE) were incubated with 20 μM IFITM3(1-

1037

108)-iEGFP for 30 min and imaged. Scale bars 20 μm. (B) Quantification of inward

1038

budding shows the percentage of GUVs prepared and treated as in (A) with at least one

1039

EGFP-positive intraluminal vesicle (ILV). Data represent mean ± SD of the results of

1040

three independent experiments, with at least 90 GUVs analyzed per sample in each

1041

experiment. (C) GUVs (99.0 mol % POPC, 0.5 mol % cholesterol, 0.5 mol % Liss-

1042

Rho-PE) were treated with 10 μM AH(56-71) and 10 μM LPC dissolved in methanol

1043

(+LPC) or the same volume of methanol (-LPC) for 30 min and imaged. Fluorescein

1044

(0.3 μM) was added to mark inward budding of GUVs. Scale bars 10 μm. (D)

1045

Quantification of inward budding showing the percentage of GUVs prepared and

1046

treated as in (C), with at least one fluorescein-containing intraluminal vesicle (ILV).

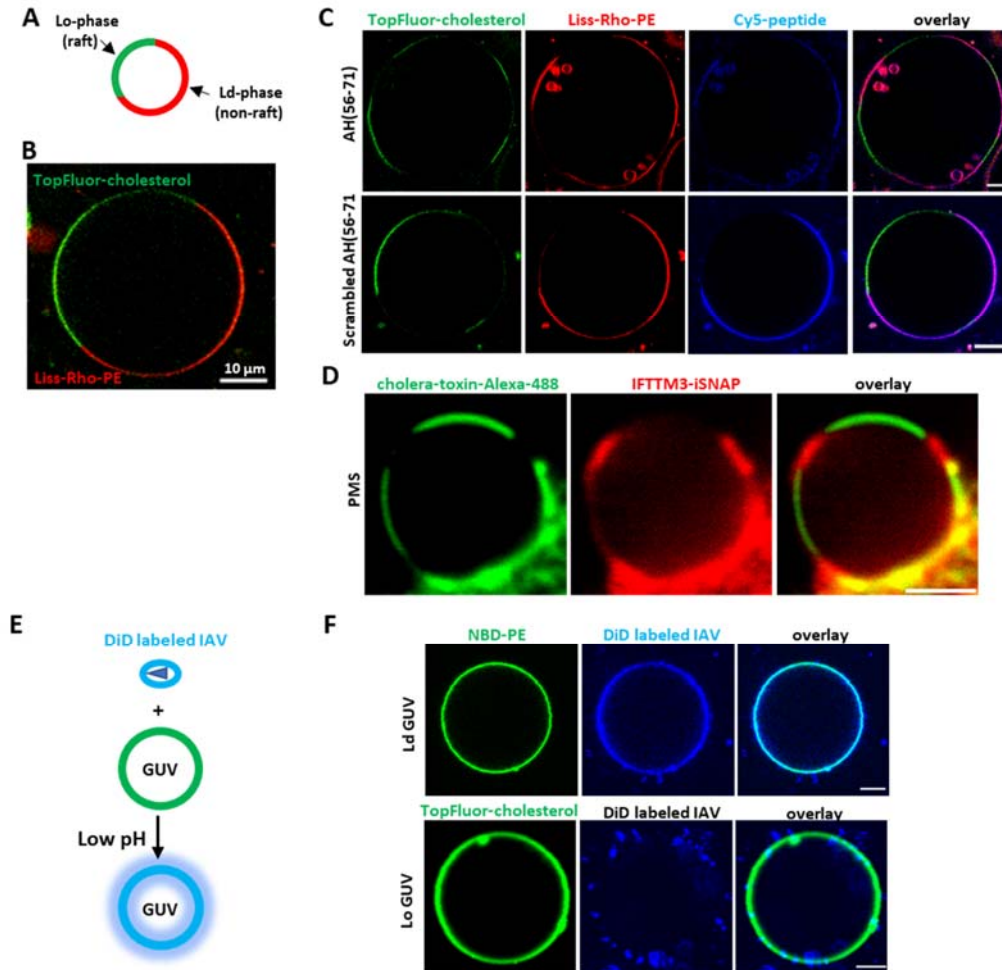
1047

Data represent mean ± SD of three independent experiments, with at least 35 GUVs

1048

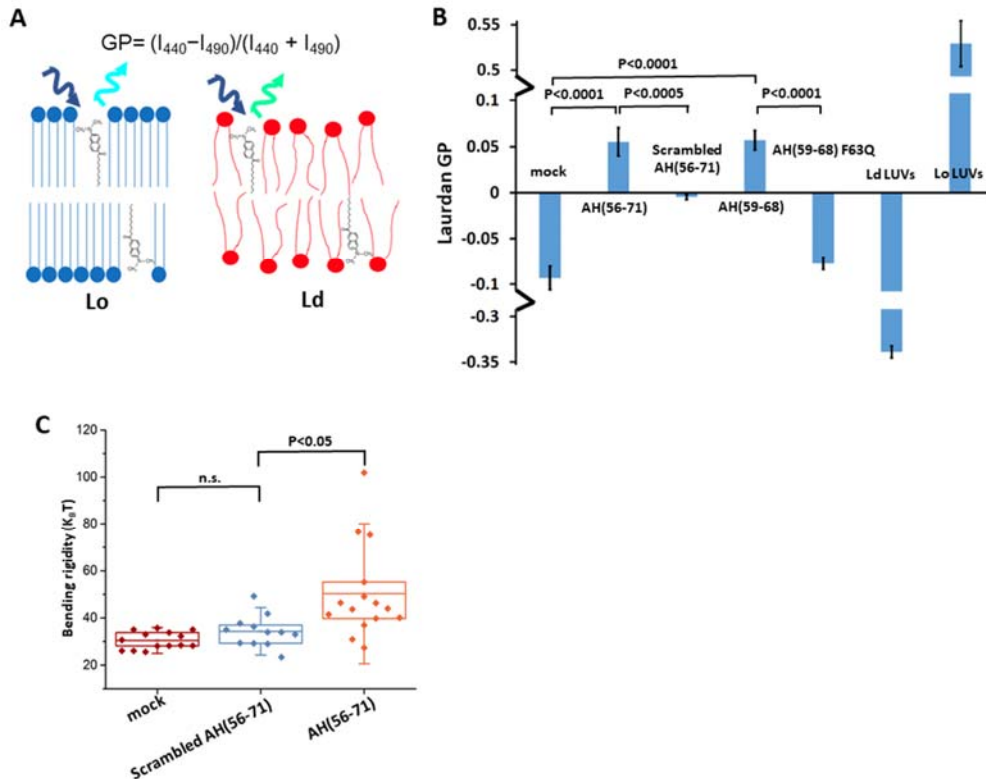
analyzed per sample in each experiment. See also Figure S3.

1049



1050

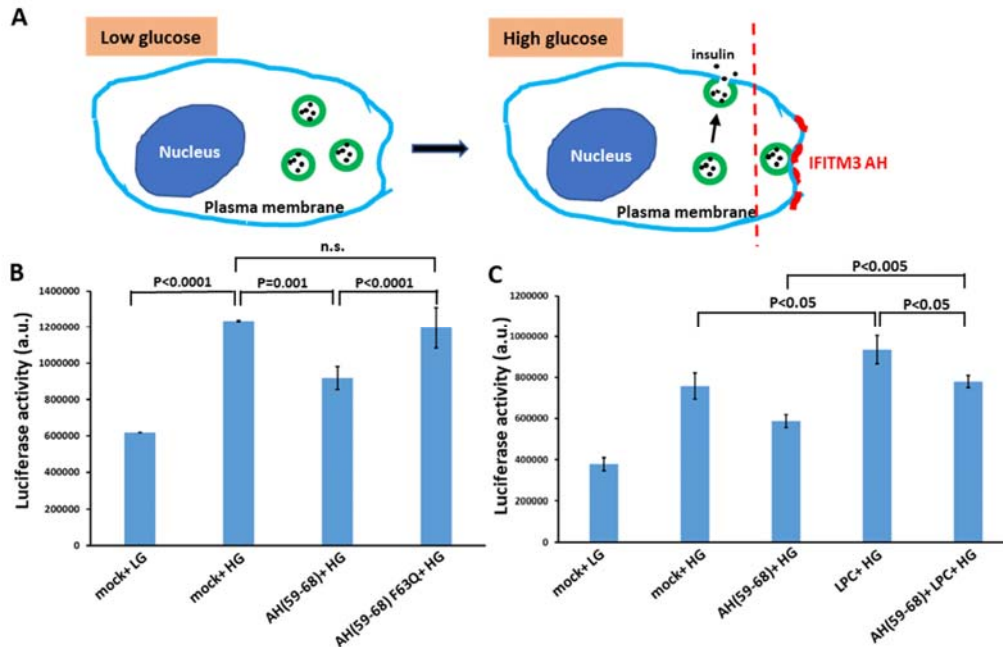
1051 **Figure 4. IFITM3 partitions into liquid-disordered membrane domains that**
 1052 **support IAV fusion.** (A) A diagram of phase-separated GUV. (B) A representative
 1053 example of phase-separated GUV containing 33.3 mol % DOPC, 33.3 mol % SM, 32.4
 1054 mol % cholesterol, 0.5 mol % TopFluor-cholesterol (marker of Lo domain) and 0.5%
 1055 Liss-Rho-PE (marker of Ld domain). (C) Phase-separated GUVs (33.3 mol % DOPC,
 1056 33.3 mol % SM, 32.4 mol % cholesterol, 0.5 mol % TopFluor-cholesterol and 0.5%
 1057 Liss-Rho-PE) were incubated with 10 μ M of Cy-5-labeled AH (56-71) or Scrambled
 1058 AH(56-71) for 30 min and imaged. Scale bars 10 μ m. (D) Plasma membrane spheres
 1059 were prepared from IFITM3-iSNAP expressing A549 cells by cell swelling. GM1 was
 1060 crosslinked with Cholera toxin B-AF488 (green) to mark the Lo phase and SNAP tag
 1061 was stained with SNAP-cell 647-SIR (red). Scale bar 2 μ m. (E) A diagram depicting
 1062 lipid mixing between DiD-labeled IAV and GUV triggered by low pH leading to DiD
 1063 dequenching. (F) Ld GUVs (top, 97.5 mol % DOPC, 2% GM1, 0.5% NBD-PE) or Lo
 1064 GUVs (bottom, 66.6 mol % SM, 30.9 mol % cholesterol, 2% GM1, 0.5 mol %
 1065 TopFluor-cholesterol) were mixed with DiD labeled IAV, lipids mixing was triggered
 1066 by addition of citrate buffer to achieve the final pH of 5.0, and samples immediately
 1067 imaged. Scale bars 5 μ m. See also Figure S4.



1068

1069 **Figure 5. IFITM3 amphipathic helix increases lipid order and stiffens membranes.**

1070 (A) A diagram illustrating the principle of Laurdan-based measurements of lipid order.
 1071 (B) Membrane binding of IFITM3 AH induces lipid ordering. Two millimoles of LUVs
 1072 (99.5 mol % POPC, 0.5 mol % cholesterol) were incubated with 25 μ M Laurdan in the
 1073 presence or absence of 40 μ M of indicated IFITM3-derived peptide at 25°C. Two mM
 1074 of Ld LUVs (99.5 mol % POPC, 0.5 mol % cholesterol, 37°C) and Lo LUVs (66.6 mol %
 1075 SM, 33.4 mol % cholesterol, 25°C) were incubated with 25 μ M Laurdan without
 1076 addition of peptide. Laurdan fluorescence was then measured at 440 and 490 nm and
 1077 the ratio was used to calculate the General Polarization (GP) of Laurdan using the
 1078 equation $GP = (I_{440} - I_{490}) / (I_{440} + I_{490})$. Data represent mean \pm SD of three independent
 1079 experiments. The statistical analysis used is the Student's t-test. (C) The membrane
 1080 bending rigidity increases in the presence of IFITM3 AH peptide. Bending rigidity
 1081 values were measured for POPC GUVs in 100 mM sucrose, 1mM HEPES at pH 7.4,
 1082 incubated with DMSO (at final concentration of \sim 0.1 v/v %; mock) or with AH(56-71)
 1083 or Scrambled AH(56-71) in DMSO at final peptide concentration of 3 nM. Every data
 1084 point corresponds to an individual vesicle. Boxes show the lower 25% and 75% quartile
 1085 around the population mean value (middle line) and error bars indicate standard
 1086 deviation.



1087

1088 **Figure 6. IFITM3 amphipathic helix inhibits membrane fusion.** (A) A diagram

1089 illustrating glucose-stimulated insulin secretion and its block by IFITM3 AH. (B)

1090 IFITM3 AH peptide inhibited glucose-stimulated insulin secretion of INS-1E cells.

1091 INS-1E cells transduced with proinsulin-luciferase fusion construct were preincubated

1092 for 5 min with 5 μ M AH(59-68) or 10 μ M AH(59-68) F63Q or same volume of DMSO

1093 (mock) and then stimulated for 20 min with high glucose (HG, 20 mM) buffer or with

1094 low glucose (LG, 2.8 mM) as control. Luciferase activity was determined by adding

1095 the coelenterazine substrate to the supernatant and reading on a Luminescence counter.

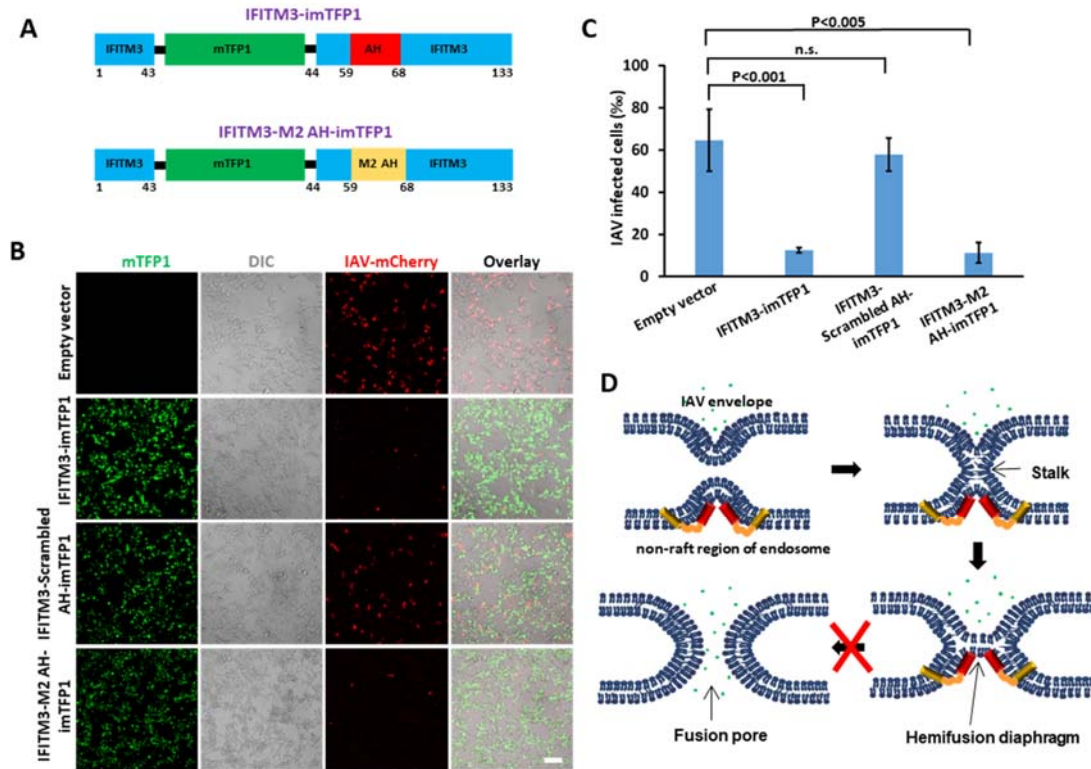
1096 Data represent mean \pm SD of the results of three independent experiments. The

1097 statistical analysis used is the Student's t-test. (C) As in (B), but for samples

1098 preincubated for 5 min with AH peptide or DMSO supplemented with 20 μ M LPC. See

1099 also Figure S5.

1100



1101

1102

Figure 7. IFITM3 amphipathic helix can be replaced by other negative curvature-

1103

inducing and lipid-ordering amphipathic helices. (A) Illustration of the internal

1104

mTFP1-tagged IFITM3 AH chimera with the Influenza virus M2 protein AH. (B)

1105

Infection assay of HEK 293T/17 cells expressing wild-type IFITM3-imTFP1, its

1106

scrambled mutant or the M2 AH chimera using mCherry-expressing IAV. Sale bar 100

1107

μm . (C) Quantification of IAV infection shown in (B). Data represent mean \pm SD of

1108

the results of three independent experiments. The statistical analysis used is the

1109

Student's t-test. Total number of cells counted are: Empty vector (3813), IFITM3-

1110

imTFP1 (3877), IFITM3-scrambled AH-imTFP1 (3525), IFITM3-M2 AH-imTFP1

1111

(4244). (D) Working model of IFITM3-mediated inhibition of IAV entry. IFITM3

1112

localizes to liquid disordered subdomains of endosomal membrane, which are the sites

1113

supporting IAV fusion, and stabilizes the hemifusion diaphragm by inducing negative

1114

membrane curvature and increasing lipid ordering and membrane stiffness. This

1115

prevents the formation of a fusion pore in the hemifusion intermediate, thus trapping

1116

IAV at a "dead-end" hemifusion stage. See also Figure S5.